TopBP1 utilises a bipartite GINS binding mode to activate the replicative helicase

Matthew Day[*2,8+], Bilal Tetik[*1], Milena Parlak[*1], Yasser Almeida-Hernández[3,4], Markus Räschle[5], Farnusch Kaschani[6,7], Heike Siegert[1], Anika Marko[1], Elsa Sanchez-Garcia[3,4], Markus Kaiser[6,7], Isabel A. Barker[2], Laurence H. Pearl[2,9+], Antony W. Oliver[2+], Dominik Boos[1+]

[1], Molecular Genetics II, Center of Medical Biotechnology, University of Duisburg-Essen, Universitätsstraße 2-5, 45141 Essen, Germany

[2], Cancer Research UK DNA Repair Enzymes Group, Genome Damage and Stability Centre, School of Life Sciences, University of Sussex, Falmer, Brighton BN1 9RQ, UK

[3], Computational Bioengineering, Fakultät Bio- und Chemieingenieurwesen, Technical University Dortmund, Emil-Figge Str. 66, 44227 Dortmund, Germany

[4], Computational Biochemistry, Center of Medical Biotechnology, University of Duisburg-Essen, Universitätsstraße 2-5, 45141 Essen, Germany

[5], Molecular Genetics, Technical University Kaiserslautern, Paul-Ehrlich Straße 24, 67663 Kaiserslautern, Germany

[6], Analytics Core Facility Essen, Center of Medical Biotechnology, University of Duisburg-Essen, Universitätsstraße 2-5, 45141 Essen, Germany

[7] Chemical Biology, Center of Medical Biotechnology, University Duisburg-Essen, Fakultät Biologie, Essen, Germany

[8] School of Biological and Behavioural Sciences, Blizard institute, Queen Mary University of London, London, E1 2AT, UK

[9] Division of Structural Biology, Institute of Cancer Research, Chester Beatty Laboratories, 237 Fulham Road, London SW1E 6BT, UK

[*] equal contribution

[+] corresponding author

Abstract

How the replicative Mcm2-7 helicase is activated during replication origin firing remains largely unknown. Our biochemical and structural studies reported here, demonstrate that the helicase activator GINS interacts with TopBP1 through two separate binding surfaces, the first involving a stretch of highly conserved amino acids in the TopBP1-GINI region, the second a surface located on TopBP1-BRCT4. The two surfaces bind to opposite ends of the A domain of the GINS subunit Psf1, and their cooperation is required for a biochemically stable TopBP1-GINS interaction. The GINI and BRCT4 domains also cooperate during replication origin firing, as revealed by immuno-replacement experiments in *Xenopus* egg extracts using different sets of mutations in either interface. Furthermore, the TopBP1-GINS interaction is incompatible with simultaneous binding of DNA polymerase epsilon to GINS when bound to Mcm2-7-Cdc45. Our TopBP1-GINS model predicts the coordination of three molecular processes, DNA polymerase epsilon arrival, TopBP1 ejection and GINS integration into Mcm2-7-Cdc45.

Introduction

Duplicating the genome accurately and exactly once each cell cycle lies at the heart of faithful genetic inheritance, with the effective execution and regulation of DNA replication origin firing being pivotal to this process. Our understanding of how origin firing in eukaryotes generates replisomes from pre-replicative complexes (pre-RCs), their inactive precursors, has recently increased. However, how the two helicase activators GINS and Cdc45 are loaded onto pre-RCs remains less well understood.

Replication initiates in two steps, origin licensing and origin firing [1]. Origin licensing generates pre-RCs in the G1 phase of the cell cycle when the activity levels of cyclin-dependent kinases (CDKs) are low [2]. The origin recognition complex (ORC), Cdc6 and Cdt1 load two hexamers of the Mcm2-7 helicase onto DNA in an ATP-dependent manner [3,4], with each hexamer forming a ring around double-stranded DNA (dsDNA). The Mcm2-7 hexamers form head-to-head double hexamers by tight interactions between their N-terminal domains. In pre-RCs, Mcm2-7 is not active as a helicase, avoiding the inappropriate generation of single-stranded DNA (ssDNA) in the G1 phase. In the following S phase, high CDK activity induces origin firing, converting each pre-RC into two bi-directional replisomes; the Mcm2-7 double hexamer separates, helicase activity is turned on, the dsDNA running inside the hexamers is unwound, and what will become the single lagging strand DNA template is excluded from each hexamer. Lagging strand extrusion enables the two now active helicases to pass each other, engaging with the DNA fork with their respective N-terminal faces [5,6].

The helicase activation step requires the loading of Cdc45 and GINS onto pre-RCs to form the CMG (Cdc45-Mcm2-7-GINS) helicase that shows robust in vitro helicase activity [7-10]. CMG assembly requires ADP-ATP exchange in the active nucleotide binding sites of the Mcm2-7

AAA ATP binding domains and occurs tightly coupled with Mcm2-7 double hexamer splitting and limited untwisting of the dsDNA inside the central CMG channels [6,11]. The subsequent extensive dsDNA unwinding, CMG bypass and assembly of mature replisomes depends on the Mcm10 protein and on many additional replisome components [6,10].

In budding yeast, Cdc45 and GINS integration requires Dbf4-dependent kinase (DDK), S-CDK, Sld3 (Treslin/TICRR in higher eukaryotes) and its constitutive partner Sld7 (MTBP), Dpb11 (TopBP1), Sld2 (RecQL4) and DNA polymerase epsilon (DNA Polε) [10,12,13]. DDK binds pre-RCs to phosphorylate the Mcm2-7 helicase, allowing Sld3-Sld7$^{\text{Treslin-MTBP}}$ association [14-16] and subsequent recruitment of Cdc45 to pre-RCs - presumably through a direct Sld3^{Treslin}-Cdc45 interaction [17]. S-CDK phosphorylates Sld3^{Treslin} on conserved CDK consensus sites, which can then bind to the N-terminal BRCT domains of Dpb11$^{\text{TopBP1}}$ [18-20] (Fig. 1a(i)). BRCT (breast cancer type 1 susceptibility) domains constitute phospho-dependent or independent protein interaction modules. The interaction between Sld3^{Treslin} and Dpb11$^{\text{TopBP1}}$ serves to recruit an additional protein complex to pre-RCs comprising GINS, Sld2$^{\text{RecQL4}}$ and DNA Polε [21]. Recruitment requires a CDK phosphorylation-mediated interaction between Sld2$^{\text{RecQL4}}$ and Dpb11$^{\text{TopBP1}}$, involving phospho-threonine 84 in Sld2$^{\text{RecQL4}}$ and the C-terminal BRCT-pair of Dpb11$^{\text{TopBP1}}$ (Fig. 1a(i)). Upon successful delivery of GINS and Cdc45, Sld2$^{\text{RecQL4}}$, Dpb11$^{\text{TopBP1}}$ and Sld3-Sld7$^{\text{Treslin-MTBP}}$ then detach from the origin-bound CMG [12,22]. DNA Polε associates with CMG in a dynamic fashion to form the CMGE complex (CMG-DNA Polε) [23]. The N-terminus of the Dpb2 subunit of DNA Polε and its vertebrate equivalent PolE2 bind to the Psf1 subunit oft GINS [24,25]. It has been suggested that this interaction represents the essential activity of DNA Polε in replication origin firing because yeast cells survive upon inactivation of DNA Polε, upon overexpression of the Dpb2 N-terminus [23].

The precise molecular mechanism underpinning how TopBP1$^{\text{Dpb11}}$, Treslin/TICRR and MTBP deliver GINS and Cdc45 to the Mcm2-7 helicase remains unclear. TopBP1$^{\text{Dpb11}}$ is a multi-BRCT domain scaffold protein containing nine BRCT domains [26]. The triple-BRCT module at the N-terminus of TopBP1$^{\text{Dpb11}}$ plus the BRCT4/5 pair share homology with budding yeast Dpb11 [27] (Fig. 1a(i)). As mentioned above, TopBP1 and Dpb11 both fulfil the task of coupling origin firing to the cell cycle via interaction with CDK-phosphorylated Treslin/TICRR$^{\text{Sld3}}$ using their respective N-terminal BRCT modules [19,20,28]. TopBP1$^{\text{Dpb11}}$-BRCT4/5 was, however, found to be non-essential to replication in *Xenopus* egg extracts [28]; perhaps surprising as the equivalent BRCT module of Dpb11$^{\text{TopBP1}}$ (BRCT3/4) mediates the essential interaction with CDK-phosphorylated Sld2 [21]. The minimal fragment of TopBP1$^{\text{Dpb11}}$ that supports replication includes BRCT0/1/2, BRCT3 (that has no equivalent in Dpb11) and a short segment C-terminal to BRCT3 termed the GINS interaction or 'GINI' region [28,29]. Yeast-two hybrid experiments have showed that the GINI regions of TopBP1 and Dpb11, which have little sequence identity, both bind to GINS [29] (Fig. 1a(i)). As both TopBP1 and Dpb11 are limiting factors for origin firing [30-32], it is likely that they are released and recycled to facilitate replication from multiple

113 different origins. It is therefore important to understand both association and disassociation
114 phases of the Dbp11^{TopBP1} interaction with GINS.
115
116 Here, we have used purified proteins to address how TopBP1^{Dpb11} loads GINS onto pre-RCs to
117 activate the Mcm2-7 helicase during replication origin firing. Our structural, biochemical, and
118 functional studies uncover the binding mode of GINS to TopBP1 and reveal an important role
119 for the TopBP1-BRCT4 domain in replication, previously thought to be dispensable. Our data
120 provide a model and framework for future investigation of CMG formation through GINS and
121 Cdc45 loading by TopBP1^{Dpb11} and the Treslin/TICRR-MTBP$^{Sld3\text{-}Sld7}$ complex. Moreover, our
122 study provides insight how TopBP1 acts at a molecular level. Such detailed understanding of
123 TopBP1^{Dpb11} is key to unravelling how this important scaffold protein can integrate its many
124 different cellular roles in chromosome biology [26].
125
126
127 **Results**
128
129 **TopBP1 interacts with GINS *in vivo* and *in vitro***
130 As previous yeast two-hybrid experiments showed an interaction of the TopBP1-GINI region
131 with Psf3 of GINS [29], we confirmed that a similar interaction could be detected in human cells.
132 Three separate proximity biotinylation experiments using cells expressing APEX2-tagged
133 TopBP1 resulted in a specific enrichment of Psf3 upon streptavidin pulldown and mass
134 spectrometry, amongst a range of other known TopBP1 interactors (Fig. 1-S1a). Psf2 was
135 detected in one experiment. Immunoprecipitation from lysates of cells transfected with
136 TopBP1-BRCT0-5 (aa, amino acids 1-766) showed a weak but specific signal for the GINS
137 subunit Sld5 (Fig. 1-S1b,c).
138
139 In addition, purified recombinant TopBP1-BRCT0-5 (TopBP1-0-5-WT) co-eluted with the GINS
140 complex from a size exclusion column at a higher apparent molecular mass, when compared
141 to either TopBP1 or the GINS complex alone (Fig. 1b; Fig. 1-S2a). Taken together, these results
142 demonstrate that an amino-terminal TopBP1 fragment spanning the BRCT repeats 0-5 (aa 1-
143 766) is sufficient to interact with GINS both *in vivo* and *in vitro*.
144
145 **Two binding motifs within TopBP1 contribute to GINS binding**
146 We then used deletion and mutation analysis to narrow down the GINS binding region within
147 the TopBP1-BRCT0-5 fragment (Fig. 1a(ii)). As expected, removing the Treslin/TICRR-binding
148 BRCT0-2 module from TopBP1 (TopBP1-ΔBRCT0/1/2) did not affect binding (Fig. 1-S2b).
149 Similarly, deletion of BRCT3 (TopBP1-ΔBRCT3) did not compromise interaction (Fig. 1c,d). In
150 contrast, deleting BRCT4/5 downstream of the GINI region (TopBP1-ΔBRCT4/5) strongly
151 impaired GINS interaction (Fig. 1e). We confirmed that the phospho-binding pocket of BRCT5
152 was not required for this interaction, using a triple point mutant that compromises its

153 phospho-binding ability (B5mut). TopBP1-B5mut bound to GINS, but interacted poorly with
154 its phosphorylated interaction partner 53BP1 [33] (Fig. 1-S2c,d).
155
156 The inability of TopBP1-ΔBRCT4/5 to bind GINS was somewhat surprising, as a similar
157 fragment of *Xenopus* TopBP1 is sufficient for interaction in yeast two-hybrid experiments and
158 able to stimulate replication in TopBP1-depleted *Xenopus* egg extracts [29]. Although initially
159 difficult to reconcile with this previous report, our observations strongly suggested that a
160 second GINS-binding motif, in addition to the GINI region, is present in the BRCT4/5 module.
161
162 **Cryo-EM structure of TopBP1-BRCT4/5 in complex with GINS**
163 To reveal how TopBP1 interacts with the GINS complex, peak fractions of TopBP1-
164 BRCTΔ0/1/2 in complex with GINS eluting from the size exclusion column (Fig. 1-S2b) were
165 applied to cryo-EM grids and movies collected on an FEI Titan Krios microscope equipped with
166 a Gatan K3 camera. A dataset comprising 18,945 movies was collected for this sample and
167 processed using a combination of CryoSPARC [34] and RELION [35] (Fig. 2-S1) to produce a final 3-
168 dimensional reconstruction, derived from 208,115 particles, at 4.6 Å based on Fourier shell
169 correlation (FSC) values. Although the resultant map was of moderate resolution due to
170 preferred orientation issues, density corresponding to the GINS tetramer could be readily
171 identified, allowing facile placement of an X-ray crystal structure by rigid-body docking
172 (PDB:9EX) (Fig. 2a). As features of the individual GINS subunits were clearly identifiable, this
173 also allowed an unambiguous orientation of the pseudo-symmetric complex. A remaining
174 section of density was too large to represent just the B domain of Psf1 (absent from the
175 docked X-ray crystal structure), but was readily accounted for by docking of the X-ray crystal
176 structure for TopBP1-BRCT4/5 (PDB:3UEN). The orientation of the two BRCT domains with
177 respect to each other was also clear from the map, arranged such that BRCT4 interacts
178 directly with the Psf1 subunit of GINS.
179
180 In the resulting model, the GINS interacting region within the BRCT repeat of TopBP1 directly
181 faces towards the A domain of Psf1 (Fig. 2a), close to where the B domain docks to the CMG
182 helicase once GINS and Cdc45 have engaged with the MCM ring. The interface includes
183 several additional amino acid residues found in the linker region connecting the A and B
184 domains, although with some ambiguity as to the precise molecular details due to the
185 resolution of the cryo-EM map (Fig. 2b). The interaction surface on BRCT4 consists of residues
186 found at the edge of the central four-stranded β-sheet, with additional interactions made by
187 residues in the loops connecting the strands; this includes amino acids between strands β3
188 and β4 that would form the second α-helix found in canonical BRCT domains but is missing
189 from the variant fold of BRCT4 [36]. Together, TopBP1-BRCT4 binds to the A domain of Psf1 and
190 involves the linker region located towards the B domain. To our knowledge, this represents a
191 novel mode for a BRCT domain-mediated interaction and ascribes for the first time a specific
192 molecular function to TopBP1-BRCT4.
193

194 Our cryo-EM model predicts that in TopBP1, amino acid residues Val590, Thr606 and Val610
195 are involved in the interface, providing a series of direct hydrophobic interactions with the
196 side chains of Trp92 and Ile97 in Psf1 (Fig. 2b). We mutated the indicated TopBP1 residues to
197 glutamate, arginine and glutamate, respectively, and tested if the resulting protein (TopBP1-
198 B4mut; Fig. 1a(ii)) co-purified with GINS. Here, TopBP1-B4mut was strongly compromised in
199 its ability to bind GINS (Fig. 2c) but could still interact with phospho-53BP1 (Fig. 2-S2a). We
200 also altered the opposing Psf1 interface by mutating Ile97 to an arginine (Psf1-I97R).
201 Recombinant Psf1-I97R bound TopBP1 weaker than the wild type protein (Fig. 2d), but could
202 still form GINS tetramers (Fig. 2-S2b).
203
204 **TopBP1 requires the conserved core of the GINI region for GINS binding**
205 As the predicted interface between the TopBP1-GINI region and Psf3 [29] was not evident in our
206 cryo-EM map we used additional interaction experiments to validate a role for this motif in
207 GINS binding. The GINI region had been loosely defined as sitting between TopBP1-BRCT3 and
208 BRCT4 (Fig. 1a(i)). A multiple amino acid sequence alignment across this region revealed a
209 high degree of conservation between vertebrate species (Fig. 3-S1a) with the section from
210 Glu484 to Tyr494 consisting of almost completely identical amino acids (Fig. 3a). We mutated
211 this core, and other regions of conservation, to generate the mutants TopBP1-Gcc (GINI
212 centre core), Gcore (GINI core) and RI-III (regions I-III) (Fig. 3a, Fig.3-S1a). Pull-down
213 experiments with these proteins revealed that TopBP1-Gcc and Gcore, but not RI-III, were
214 compromised in GINS interaction (Fig. 3b). Secondary structure prediction and AlphaFold2
215 models of TopBP1 suggested the presence of a short helix within this core region for some
216 vertebrate species. By mutation of the central leucine-leucine motif to two consecutive
217 prolines to break the helix (TopBP1-Gpp; Fig. 3a) we could show that the interaction with GINS
218 was strongly compromised, with no effect on binding to 53BP1 (Fig. 3-S1b; Fig. 2-S2a). To test
219 if this helix contributed to a GINS-interaction surface, we used fluorescence polarisation (FP)
220 to measure interaction between a fluorescently labelled GINI-core peptide (aa Ala478-
221 Gly497) and the GINS tetramer, determining a dissociation constant K_d of ~8 µM (Fig. 3c). A
222 fluorescently labelled peptide harbouring the PP mutation failed to bind (Fig. 3c). We
223 therefore concluded that the GINI region is a *bona fide* GINS interaction site in its own right,
224 but with only moderate binding affinity.
225
226 **The GINI-core helix binds Psf1 and 3**
227 We next sought to identify and confirm the site in GINS that interacts with the TopBP1-GINI
228 region. Structural prediction using the multimer mode of AlphaFold2 suggested that the GINI-
229 core helix interacted with the distal part of the Psf1 A domain (Fig. 3-S1c). In parallel, we also
230 used 'blind' molecular docking simulations with the GINI core region (487-DEDLLSQY-494) to
231 identify candidate binding sites on the GINS tetramer. Pleasingly, the resultant docking
232 calculations were consistent with the results obtained from AlphaFold, with solutions
233 amongst the top-10 candidates clustering in a binding site in close proximity (Fig. 3-S1d-g).
234

235 To validate the predictions, we performed a BS3-crosslinking mass spectrometry experiment
236 with purified recombinant TopBP1-GINS complex. The detected crosslinks confirmed
237 proximity of the TopBP1-GINI region and the Psf1-A domain, close to the site where the GINI-
238 core helix (residues 487-494) was predicted to contact the A domain. Several GINI-core-
239 proximal residues crosslinked with Lys63 and Thr61 of the Psf1 (Fig. 3-S2a); both crosslinked
240 Psf1 residues are situated at the distal end of the Psf1 A domain (Fig. 3-S2b,c). The GINI-core-
241 proximal residues also crosslinked with lysines 74 and 80 of Psf3; each Psf3 residue also being
242 in close proximity to the predicted site of interaction. Given that the GINI-core helix itself
243 contains no lysine residues, our data are consistent with the hypothesis that the GINI-core
244 helix binds to both the distal region of the Psf1 A domain and the adjacent region of Psf3 (see
245 Fig. 3-S2 for detailed description).
246
247 With this information in hand, we sought to improve the overall resolution of our cryo-EM
248 data, to provide additional evidence for the mapped TopBP1-GINI/GINS interaction. A sample
249 produced using an alternative GINS-expression construct that omits the Psf1 B domain served
250 to improve detail around the predicted interaction region (Fig. 3-S3). The resultant map
251 allowed a short helical element, consistent with the AlphaFold2 multimer predictions, to be
252 incorporated into our model (Fig. 3d).
253
254 The hydrophobic side of the amphipathic GINI-core helix can be seen to pack across two
255 helices of the Psf1-A domain, making interactions with the side chains of Leu490 and Leu491
256 of the GINI region and Val47, Lys51, Ile59, Ile62, Lys63 and His66 of Psf1. Additionally, the
257 sidechain of Tyr494 in the GINI region is inserted into a small pocket on the surface of Psf1
258 formed by Tyr40, Asn43 and Leu69 with the hydroxyl group picking up a hydrogen bond with
259 the side chain of His66.
260
261 For validation, we mutated two separate pairs of residues in Psf1 that appeared critical for
262 TopBP1-GINI interaction: Asn43/Lys51, and Lys63/His66. Both pairs were exchanged for
263 alanine and glutamate to yield Psf1-NK43/51AE and Psf1-KH63/66AE, respectively. One
264 residue of each pair forms part of the pocket accepting Tyr494 from the GINI region, whilst
265 Lys51 and Lys63 are positioned such that they could form salt bridges with either Asp487 or
266 Glu495 as well as forming part of the hydrophobic grove that accommodates the leucines of
267 the GINI-core helix. As Psf1-KH63/66AE failed to produce a GINS tetramer it was excluded
268 from future experiments. In contrast, Psf1-NK43/51AE readily formed the tetramer (Fig. 2-
269 S2b) but was severely compromised in its ability to interact with TopBP1-BRCT0-5-WT (Fig.
270 3e) again consistent with binding of the GINI region to the distal end of the Psf1 A domain
271 and the adjacent regions in Psf3.
272
273 **Cooperation between the GINI core region and BRCT4**
274 Our interaction studies demonstrate that both the GINI region and BRCT4 domain of TopBP1
275 are individually required to form a biochemically stable interaction with GINS. This suggests a

276 model in which both interactions have relatively moderate binding affinities, but cooperate
277 to form a composite interaction surface with high avidity. Consistent with this notion,
278 estimations of binding free energies suggests that affinities are lower when the surfaces
279 interact individually rather than simultaneously (Fig. 4a). The moderate binding affinity
280 determined for the GINI-core peptide measured by FP is consistent with this cooperative
281 binding model (Fig. 3c).
282
283 We moved on to ask if the GINI and BRCT4 regions cooperate to support DNA replication, by
284 testing if defined mutations in TopBP1 (Fig. 4b) could suppress replication in *Xenopus* egg
285 extracts. Immunodepleting TopBP1 with two independent antibodies (anti-TopBP1-#1 and
286 #2) effectively removed the endogenous protein from extracts (Fig. 4c), producing a strong
287 reduction in radioactive α-^{32}P-dCTP incorporation when compared to a 'mock' IgG depletion
288 control (Fig. 4d). Add-back experiments using recombinant TopBP1-BRCT0-5-WT effectively
289 rescued replication (Fig. 4d), whereas addition of either TopBP1-BRCT0-5-Gcc or TopBP1-
290 BRCT0-5-Gpp (Fig. 3a) showed moderate reductions in replication when compared with WT
291 (Fig. 4e, Fig. 4-S1a). TopBP1-ΔBRCT4/5 (GINI domain intact, Fig. 1a) was not detectably
292 compromised in its ability to support replication, consistent with previous observations [28,29].
293 TopBP1-B4mut behaved in a similar fashion (Fig. 4-S1b). However, combining deletion of
294 BRCT4/5 or the B4mut mutation with either TopBP1-BRCT0-5-Gcc or -Gpp reduced replication
295 to nearly background levels (Fig. 4e, Fig. 4-S1). These results indicate that add-back of wild-
296 type TopBP1 to depleted *Xenopus* egg extracts supports DNA replication at close to
297 physiological levels, and that whilst the presence of either a functional GINI or BRCT4 region
298 is sufficient to support replication, this is not as effective as adding the fully wild-type protein.
299
300 We next tested if the TopBP1-GINS interaction is required for the origin firing step of
301 replication. We isolated chromatin from *Xenopus* egg extracts after immuno-depletion and
302 add-back of TopBP1-BRCT0-5-WT or mutants, following a 75-minute incubation period. To
303 increase signal, we added aphidicolin, preventing termination and allowing replisomes to
304 accumulate on chromatin. Mass spectrometry using the CHROMASS protocol [37] and
305 immunoblotting showed geminin-sensitive chromatin binding of Mcm2-7 subunits
306 irrespective of whether buffer or recombinant TopBP1-BRCT0-5-WT was added, indicating
307 that licensing occurs independently of TopBP1 status (Fig. 5, Fig. 5-S1). Several replisome
308 markers, including GINS and Cdc45, were detected on chromatin in extracts containing
309 TopBP1-WT, but were significantly reduced when buffer or the TopBP1-Gcc-ΔBRCT4/5
310 mutant were added. Thus, the GINS binding sites in TopBP1 are required for origin firing
311 (replisome formation) upstream of CMG formation. Immunoblotting of chromatin samples
312 upon complementation with the single mutants TopBP1-Gcc and TopBP1-ΔBRCT4/5 showed
313 strong and mild replication defects, respectively, similar to their effects in replication analyses
314 at similar time points (Fig. 4e, Fig. 4-S1). We conclude that the BRCT4 and the GINI regions
315 cooperate to assemble the CMG helicase.
316

Mutually exclusive binding of TopBP1 and DNA Polε to GINS in the context of CMG

We next wanted to know how the TopBP1 interaction with GINS relates to the integration of GINS in the CMGE helicase. Analysis of the human CMG structure revealed that both binding sites for TopBP1 in GINS are accessible for protein interaction (Fig. 6a) [25]. However, the binding of DNA Polε and TopBP1 are mutually exclusive. Although the direct binding sites on GINS for PolE2 and for TopBP1 do not overlap, superposition of CMG bound to DNA Polε and TopBP1 revealed major steric clashes between TopBP1 and PolE2 (Fig. 6b,c). Thus, TopBP1 must leave the CMG complex before PolE2 associates.

Comparison of the GINS structures in different contexts revealed interesting conformational changes of the Psf1-B domain. The Psf1-B domain is not required for forming the GINS tetramer but is involved in CMG formation [38]. Cryo-EM data of the GINS tetramer alone suggests that the B domain is flexible because the B domain could not be detected at the same contour level as the rest of the GINS complex (Fig. 6-S1a). This is consistent with the reported 'invisibility' of the B domain in a previous crystallization study of GINS [39]. The B domain apparently retains similar flexibility in the TopBP1-GINS complex as it is not resolved in our BRCT4-GINS structure (Fig. 6-S1b). In contrast, previous cryo-EM evidence [25] suggested that the Psf1-B domain adopts a discrete conformation in the CMG context. It appears to become ordered through its packing against Cdc45 (Fig. 6a). In this conformation, the B domain binds to the N-terminus of PolE2 once DNA Polε associates to form CMGE.

These observations suggest that the Psf1-B domain reconfigures from a flexible state into a well-ordered state upon CMG assembly. TopBP1-BRCT4 must then dissociate to exchange with DNA Polε for CMGE formation. Once CMG has formed DNA Polε seems to dynamically associate with CMG [23]. Together, these observations suggest that the three processes 1) handover of GINS from TopBP1 to pre-RCs, 2) DNA Polε association and 3) TopBP1 ejection may be mechanistically intertwined.

Discussion

Relevance

Our data provide an understanding of the interaction between TopBP1^{Dpb11} and GINS at the molecular level, and how this supports replication origin firing. Recent insight into origin firing has largely come from studies focussed on understanding how the yeast Mcm2-7 helicase operates as a molecular machine to build replication forks [1,6,10,11,13,15,16,40-43], however these studies have rarely investigated how the helicase is activated by loading of GINS and Cdc45 in order to form the CMG complex. Our approach here, provides a first detailed glimpse into how TopBP1^{Dpb11} may load GINS onto pre-RCs.

357 Formation of the CMG complex serves as a key regulatory step of origin firing. In metazoa and
358 yeast, CMG formation involves the signal integrators Treslin/TICRR/Sld3, MTBP/Sld7,
359 RecQL4/Sld2, TopBP1/Dpb11 and the Mcm2-7 helicase itself. Apart from coupling origin firing
360 to the S phase, these signal integrators are targeted by the DNA damage checkpoint and other
361 regulatory pathways to mediate DNA damage-dependent origin firing control, execution of
362 the temporal replication program and fine-tuning of origin firing [44-55 56-58]. Such regulation
363 helps avoid replication stress that is key to structural and numerical chromosomal instability
364 in cancer cells [59].
365
366 **The molecular role of TopBP1 in S phase-specific CMG formation**
367 Like yeast Dpb11, TopBP1 is a scaffold protein that couples origin firing to S phase of the cell
368 cycle (S-phase coupling). For this, the N-terminal triple BRCT0-2 module of TopBP1 binds
369 Treslin/TICRR^{Sld3}, in a strictly phospho-dependant manner, via two CDK sites that are which
370 are also conserved in the equivalent budding yeast protein Sld3^{Treslin} [19,20]. Despite this level of
371 conservation, some aspects of origin firing in vertebrates are likely to have changed
372 mechanistically when compared to the yeast paradigm: 1) It is known that DDK strengthens
373 the interaction between TopBP1^{Dpb11} and the Treslin/TICRR-MTBP$^{Sld3-Sld7}$ complex, albeit via
374 an unclarified mechanism [60], whereas a similar role for DDK in the equivalent Dpb11/Sld3-
375 Sld7 interaction has not been reported. 2) an N-terminal fragment that excludes the BRCT4/5
376 module of TopBP1^{Dpb11} effectively supports replication in *Xenopus* egg extracts [29 28], whereas
377 the equivalent BRCT3/4 module of Dpb11^{TopBP1} is essential, as it is required for binding to
378 Sld2^{RecQL4} phosphorylated by S-CDK [21]. These mechanistic differences therefore exemplify
379 evolutionary flexibility in S-phase coupling, supported by findings in the *C. elegans* and fission
380 yeast model organisms where the contributions of Treslin/TICRR^{Sld3} and RecQL4^{Sld2}
381 equivalents have changed during evolution [61,62]. Such flexibility may be supported by the
382 partial redundancy of S phase kinases (S-CDK and DDK) and their substrates (Treslin/TICRR^{Sld3},
383 RecQL4^{Sld2}, Mcm2-7).
384
385 It is known that TopBP1^{Dpb11} supports CMG formation via an interaction with the GINS
386 complex. In budding yeast, Dpb11^{TopBP1} and GINS are recruited to pre-RCs as part of a 'pre-
387 loading complex' (pre-LC) comprising Dpb11^{TopBP1}, GINS, DNA Polε and Sld2^{RecQL4} [63].
388 Dpb11^{TopBP1} appears to 'dock' the pre-LC onto Sld3^{Treslin}-Sld7^{MTBP}-Cdc45 via a CDK-mediated
389 Dpb11^{TopBP1}-Sld3^{Treslin} interaction; DDK is required for initial binding of Sld3^{Treslin}-Sld7^{MTBP}-
390 Cdc45 onto pre-RCs [13,41]. However, the pre-LC complex containing TopBP1^{TopBP1} and GINS has
391 not been characterized in detail in metazoa.
392
393 The GINI region of TopBP1^{Dpb11}, broadly defined as the region between BRCT3 and BRCT4,
394 bound to Psf3 in Y2H experiments [29]. Its functional relevance was demonstrated by
395 experiments using a truncated TopBP1^{Dpb11} fragment lacking the GINI region, which only
396 poorly supported replication [29]. We show here that a short alpha-helix found at the core of
397 the conserved GINI region (GINI-core helix) forms an essential part of the binding surface

398 necessary and sufficient for detectable interaction with GINS. Moreover, this helix cooperates
399 with a second binding site situated in BRCT4 to form a composite high-affinity GINS-
400 interaction surface; involving a hereinto unknown mode of BRCT-interaction. Notably, our *in*
401 *vitro* experiments show that each individual site is insufficient to form a biochemically stable
402 complex with GINS, but are able to support significant levels of replication in *Xenopus* egg
403 extracts, suggesting that even a low affinity TopBP1^{Dpb11}-GINS interaction is sufficient to allow
404 origin firing. We rationalise this statement by suggesting that *in vivo*, contacts between other
405 pre-LC components may compensate for a weakened TopBP1^{Dpb11}-GINS interaction. Whilst
406 neither the GINI region nor BRCT4 are required individually for origin firing, their combined
407 action is essential, suggesting that neither site has a unique molecular role beyond GINS
408 binding. The simplest scenario is that their common essential molecular role is to chaperone
409 GINS onto pre-RCs, and that the partial redundancy between the two binding sites provides
410 an explanation for why the role of TopBP1^{Dpb11}-BRCT4/5 in replication has gone unrecognised.
411
412 Consistent with published Y2H experiments [29], our structural data indicate that the GINI core
413 helix region interacts with both Psf1 and Psf3, at a position close to the distal end of the Psf1
414 A domain, whereas BRCT4 interacts with both the base of the Psf1-A domain and the linker
415 that connects it to the B domain. Notably, both receiving interfaces are fully accessible in the
416 context of either the unbound GINS tetramer or in the CMG complex, consistent with a model
417 where TopBP1^{Dpb11} recruits GINS using both motifs (Fig. 6-S2). TopBP1^{Dpb11} may
418 simultaneously bind phosphorylated Treslin/TICRR^{Sld3}-MTBP^{Sld7} via its N-terminal BRCT0-3
419 module [19,20,64], with Treslin/TICRR^{Sld3} bringing Cdc45 along through its Sld3-Treslin homology
420 domain [17,65]. One open question in the field is the biological role of the BRCT3 domain in
421 TopBP1, which has no equivalent in Dpb11. We speculate here, that it might function to bind
422 a yet undescribed essential metazoan-specific origin firing factor.
423
424 After delivery of Cdc45, the subsequent release of TopBP1^{Dpb11} and Treslin/TICRR^{Sld3}-MTBP^{Sld7}
425 is also likely to be important, as presumably they must be 'recycled' to allow the use of late
426 firing origins [32]. However, such a release mechanism remains unclear. The low affinities of the
427 two individual GINS-interacting sites in TopBP1^{Dpb11}, offers the idea that release of one site,
428 in a 'zipper'-like fashion, would significantly destabilise the complex to trigger dissociation. In
429 the context of the CMG, there is no obvious steric clash that would force TopBP1^{Dpb11}
430 dissociation, however this is not true for CMGE, where binding of DNA Polε would be
431 incompatible, suggesting that the two proteins exchange. Whether TopBP1^{Dpb11} dissociation
432 is a prerequisite for DNA Polε association, or whether the polymerase acts to displace
433 TopBP1^{Dpb11} remains unclear; the important but mechanistically unclear role of DNA Polε in
434 CMG formation therefore remains open [23,24]. The reconfiguration of the Psf1-B domain during
435 CMG formation suggests another potential mechanism for TopBP1 release. The B domain
436 seems flexible in the TopBP1-GINS complex and establishes an extensive set of interactions
437 with Cdc45 when it reconfigures to form CMG, which might favour Polε binding over

438 TopBP1^{Dpb11}-BRCT4. The action of phosphatases could also potentially release the entire
439 Treslin/TICRR^{Sld3}-MTBP^{Sld7}-TopBP1^{Dpb11} complex from pre-RCs [66].
440
441 Recent insights have suggested that formation of the CMG complex is tightly associated with
442 (i) splitting of Mcm2-7 double hexamers into single hexamers; (ii) the exchange of ADP for
443 ATP in the Mcm2-7 nucleotide-binding sites; and (iii) limited unwinding of dsDNA inside the
444 central channels of the split, single hexamers [6,11]. How TopBP1, Treslin/TICRR and MTBP
445 relates to these steps will be key to understanding whether their mechanistic roles go beyond
446 just a simple chaperoning function, guiding Cdc45 and GINS to pre-RCs. For example, the
447 reported homo-dimerization of TopBP1 and MTBP might play a role in the cooperative
448 conversion of Mcm2-7 hexamers into replisomes, thus guaranteeing bi-directional
449 replication[60,67].
450
451 Taken together, our data provide insight into, and a testable hypothesis for, the series of
452 molecular events leading to CMGs formation. Additional studies will be required to
453 understand more fully its regulation by the cell cycle, as well as DNA damage and other
454 pathways; potentially leading to future therapeutic routes for the treatment of cancer, due
455 the high reliance of tumours on high levels of replication initiation [68]. Targeted interference
456 with origin firing, which benefits from a molecular understanding of the process, could be one
457 potential avenue, consistent with the testing of DDK inhibitors as candidates in clinical trials
458 [69].
459

460 # Methods
461
462 ## Antibodies
463

name	Antigen/source
Anti-DB4	TopBP11-360, rabbit, self-made
Anti Sld5	Sld5/Rabbit, self-made
Anti-Flag	Flag peptide, mouse
Anti-53BP1	53BP1, rabbit
Anti-Myc	Myc tag, mouse
Anti-TopBP1 #1	XTopBP1 1-365, rabbit, self-made
Anti-TopBP1 #2	XTopBP1 999-1299, rabbit, self-made
Anti-XCdc45	XCdc45/ rabbit, self-made
Anti-XSld5	XSld5, rabbit, self-made
Anti-XPolE2	XPolE25, rabbit, self-made
Anti-Mcm6	Mcm6 775-821/ rabbit, BETHYL A300-194A
Anti-Mcm4	Mcm4 750-850/ rabbit, Abcam ab4459

464
465
466 ## DNA plasmids
467

plasmid name	vector backbone	recombinant protein
BT702	pLib	TopBP1-766 LL489/490PP-Strep
BT707	pLib	TopBP11-766-Strep
BT708	pLib	TopBP11-766 RegionI-Strep
BT709	pLib	TopBP11-766 RegionII-Strep
BT710	pLib	TopBP11-766 RegionIII-Strep
BT711	pLib	TopBP11-766 Gcore-Strep
BT712	pLib	TopBP11-766 Gcc-Strep
BT735	pLib	TopBP11-766 SKK654/661/704VRE-Strep
BT759	pLib	TopBP11-549-Strep
BT760	pLib	TopBP11-549 Gcc-Strep
BT761	pLib	TopBP11-549-LL489/490PP-Strep
BT770	pLib	TopBP11-766 B4mut-Strep
BT772	pLib	TopBP11-766Gcc/B4mut-Strep
BT805	pLib	6xHis-3xFlag-Sld5
BT806	pLib	Psf1
BT807	pLib	Psf2
BT808	pLib	Psf3
BT781	pLib	Psf1 NK43/51AE
BT782	pLib	Psf1 KH63/66AE
MD106	pBIG1a	Psf1 Psf2 Psf3 6xHis-3xFlag-Sld5
MD101	pLib	Psf1(1-151)
MD107	pBIG1a	Psf1(1-151) Psf2 Psf3 6xHis-3xFlag-Sld5
MD146	pET17b	HIS-TopBP1(1-766)-Strep
MD147	pET17b	HIS-TopBP1(331-766)-Strep

468
469 **Purification of TopBP1(331-766) for structural studies**
470 TopBP1(1-766)-Strep was transferred into a pET17 vector, in order to add a HIS tag to aid
471 purification and allow for bacterial expression, using NEBuilder (NEB, Hitchin, UK). A plasmid
472 encoding HIS-(3C)-TopBP1(331-766)-Strep was transformed into BL21(DE3) cells, grown in
473 TurboBroth at 37 °C to an OD600 of 2.0 and induced by the addition of 0.5 mM IPTG prior to
474 overnight incubation at 16 °C. Cell pellets were re-suspended in lysis buffer containing 25 mM
475 HEPES pH 7.5, 200 mM NaCl, 0.5 mM TCEP, and supplemented with 10 U DNASE Turbo and
476 cOmplete, EDTA-free Protease Inhibitor Cocktail (Merck), then disrupted by sonication,
477 and the resulting lysate clarified by centrifugation at 40,000 x g for 60 min at 4°C. The
478 supernatant was applied to a 5mL HiTrap TALON crude column (GE Healthcare, Little Chalfont,
479 UK), washed first with lysis buffer, followed lysis buffer supplemented with 10 mM imidazole,
480 with any retained protein then eluted by application of the same buffer supplemented with
481 250mM imidazole. The eluted protein was diluted with lysis buffer before application to a
482 5mL HiTrap STREP column (GE Healthcare, Little Chalfont, UK), washed with lysis buffer and
483 eluted using buffer supplemented with 2 mM desthiobiotin. The eluate was concentrated
484 before application to a Superdex200increase 10 300 column (GE Healthcare, Little Chalfont,
485 UK) equilibrated in 10 mM HEPES pH 7.5, 150 mM NaCl, 0.5 mM TCEP.
486
487 **Purification of TopBP1-BRCT0-5-Strep for interaction and *Xenopus* egg extract studies**
488 Sf9 insect cells were grown as suspension culture in insect cell media (Pan biotech, P04-850
489 500) at 27°C. Baculoviruses were generated using pLIB-based constructs (Addgene, 80610).
490 500 ml Sf9 cells (1x106/ml) were infected with a 1:100 dilution of recombinant baculovirus
491 carrying an expression construct for TopBP1-1-766-Strep-WT or mutants, and were incubated
492 at 27°C for 72 h. Cell pellets were lysed by douncing in 30 ml of lysis buffer (20 mM HEPES pH
493 8.0, 150 mM NaCl, 0.1% (v/v) Tween-20, 0.5 mM TCEP, protease inhibitor cocktail (Roche
494 Complete protease inhibitor cocktail, 05056489001)). The lysate was centrifuged at 44800 g
495 for 45 min and the supernatant was loaded onto the StrepTrapHP-1ml column (Cytiva,
496 28907546) using an Äkta FPLC system. The bound protein was eluted with elution buffer (20
497 mM HEPES pH 8.0, 150 mM NaCl, 0.01% Tween-20 (v/v), 0.5 mM TCEP, 2% (v/v) glycerol, 2.5
498 mM desthiobiotin).
499
500 **Purification of GINS from insect cells for structural and fluorescence polarisation studies**
501 Truncations of Psf1 were made using a Q5 Site-Directed Mutagenesis Kit (NEB, Hitchin, UK).
502 Psf1 Psf2 Psf3 HIS-(3C)-Sld5 or Psf1(1-151) Psf2 Psf3 HIS-(3C)-Sld5 were expressed from a
503 single baculovirus produced through combing the individual pLib vectors into pBig1a
504 (referecene for biGBac). Plasmids were transformed into DH10BAC cells (Fisher Scientific, UK)
505 and bacmids were purified by standard procedures. Bacmids were transfected into SF9 cells
506 (Thermofisher, UK) using Cellfectin II reagent (Fisher Scientific, UK), before viral amplification
507 and protein expression. Cell pellets were re-suspended in lysis buffer containing 25 mM
508 HEPES pH 7.5, 200 mM NaCl, 0.5 mM TCEP, and supplemented with 10 U DNASE Turbo and

509 cOmplete, EDTA-free Protease Inhibitor Cocktail (Merck), then disrupted by sonication, and
510 the resulting lysate clarified by centrifugation at 40,000 x g for 60 min at 4°C. The supernatant
511 was applied to a 5mL HiTrap TALON crude column (GE Healthcare, Little Chalfont, UK),
512 washed first with lysis buffer, followed lysis buffer supplemented with 10 mM imidazole, with
513 any retained protein then eluted by application of a gradient up to 250mM imidazole. Peak
514 fractions were pooled and concentrated before application to size exclusion chromatography.
515 For aSEC and EM experiments a Superdex200increase 10 300 column (GE Healthcare, Little
516 Chalfont, UK) equilibrated in 10 mM HEPES pH 7.5, 150 mM NaCl, 0.5 mM TCEP was used
517 while for FP experiments a Superdex200 16 600 column (GE Healthcare, Little Chalfont, UK)
518 equilibrated in 25 mM HEPES pH 7.5, 150 mM NaCl, 1 mM EDTA, 0.25 mM TCEP, 0.02 % (v/v)
519 Tween 20 was used.
520
521 **Purification of GINS from insect cells for pulldown experiments**
522 Sf9 insect cells cultured as described above were co-infected with 1:50 dilution of each four
523 recombinant baculoviruses for expressing 6xHis-3xFlag-Sld5, Psf1, Psf2 and Psf3, respectively.
524 72 h post infection, pellets from one litre cells were lysed by douncing in 60 ml of lysis buffer
525 (20 mM HEPES pH 8.0, 300 mM NaCl, 0.1% (v/v) Tween-20, 25 mM imidazole, 0.5 mM TCEP,
526 protease inhibitor cocktail (Roche Complete protease inhibitor cocktail, 05056489001)). The
527 lysate was centrifuged at 44800 g for 45 min and the supernatant was incubated with 2.5 ml
528 Ni-NTA agarose beads (Qiagen,30210) for 1 h at 4°C. The bound protein was eluted with six
529 bead volumes elution buffer (20 mM HEPES pH 8.0, 300 mM NaCl, 0.01% (v/v) Tween-20, 250
530 mM imidazole, 0.5 mM TCEP, 2% (v/v) glycerol). The eluate was dialysed into 20 mM HEPES
531 pH 8.0, 150 mM NaCl, 0.01% (v/v) Tween-20, 0.5 mM TCEP, 2% (v/v) glycerol, and then applied
532 onto an HiTrap HP Q anion exchange column (Cytiva, 17115301). To elute the bound protein,
533 a linear gradient of NaCl (from 150 mM to 1 M) in elution buffer (20 mM HEPES pH8.0, 0.01%
534 (v/v) Tween-20, 0.5mM TCEP, 2% (v/v) glycerol) was used. Peak fractions including GINS were
535 pooled and loaded onto gel filtration column (running buffer: 20 mM HEPES pH8.0, 300mM
536 NaCl, 0.01% (v/v) Tween-20, 0.5mM TCEP, 2% (v/v) glycerol).
537
538 **Purification of geminin**
539 GST tagged *Xenopus* geminin (Xgeminin) in pGEX was purified from 6 l of Rosetta E. coli
540 culture. Expression of GST-Xgeminin was induced with 1 mM IPTG at OD600 = 0.8 at 25 °C
541 over night. Cells were harvested by centrifugation at 6000 rpm (JLA-8.1, Avanti JXN-26
542 Beckman Culture) for 15 min. Subsequently, cells were resuspended in lysis buffer (5 mg/ ml
543 lysozyme, 20 mM Hepes pH 7.7, 200 mM NaCl, 5 mM β-mercaptoethanol, 5 % glycerin) and
544 lysed by sonication. Cell suspension was centrifuged at 20000 rpm (SS-34, Sorvall RC 6 PLUS)
545 for 20 min at 4 °C. Supernatant was incubated with glutathione-sepharose (GE Healthcare
546 17513201) for 3 h before elution with lysis buffer + 50 mM glutathione (Applichem
547 A2084,0025=. Peak fractions were pooled and dialyzed into XBE2 buffer (100 mM KCl, 2 mM
548 MgCl2, 0.1 mM CaCl2, 1.71 % w:v sucrose, 5 mM K-EGTA, 10 mM HEPES-KOH, pH 7.7) and
549 concentrated to 360 µM Xgeminin. Aliquots were frozen at - 80 °C.

550
551 **Size exclusion chromatography**
552 TOPBP1 and GINS constructs were mixed in an equimolar ratio to give a final concentration
553 of 20 µM of each component and incubated on ice for at least 30 minutes prior to application
554 to a Superdex200increase 10 300 column (GE Healthcare, Little Chalfont, UK) equilibrated in
555 10 mM HEPES pH 7.5, 150 mM NaCl, 0.5 mM TCEP.
556
557 **Fluorescence polarisation experiments**
558 Fluorescein-labelled peptides (WT: 'Flu'-GYGAPSEKHEQADEDLLSQYENG or LLPP: 'Flu'-
559 GYGAPSEKHEQADEDPPSQYENG) (Peptide Protein Research Ltd, Bishops Waltham, UK) at a
560 concentration of 100nM, were incubated at room temperature with increasing
561 concentrations of GINS in 25 mM HEPES pH 7.5, 150 mM NaCl, 1 mM EDTA, 0.25 mM TCEP,
562 0.02 % (v/v) Tween 20 in a black 96-well polypropylene plate (VWR, Lutterworth, UK).
563 Fluorescence polarisation was measured in a POLARstar Omega multimode microplate reader
564 (BMG Labtech GmbH, Offenburg, Germany). Binding curves represent the mean of 3
565 independent experiments, with error bars of 1 standard deviation.
566
567 **Immunoprecipitations from transiently transfected 293T cells**
568 Transient transfections of 293T cells (ATCC CRL-11268) were carried out as described using
569 PEI (polyethyleneimine) according to a protocol kindly shared by David Cortez' lab. 4 µg
570 plasmid DNA in 100 µl DMEM (Thermofisher, 41965039) without penicillin-streptomycin were
571 combined with 2.4 µl Polyethylenimin (Sigma, 408727; 10 mg/ml) and incubated for 20
572 minutes before addition to 4 x 106 cells on a 10 cm dish. Transfected cells were used 72 h
573 post transfection.
574 6xMyc-Tev2-TopBP1 was immunoprecipitated from native lysates of transiently transfected
575 293T cells. 72 h post transfection, 293T cells were lysed by douncing in ten times cell pellet
576 volume of lysis buffer (20 mM HEPES pH8.0, 150mM NaCl, 0.1 % (v/v) Tween-20, 0.5mM TCEP,
577 2% (v/v) glycerol, protease inhibitor cocktail (Roche, Complete protease inhibitor cocktail,
578 05056489001)), and centrifuged at 20000 g for 15 min at 4 °C. The soluble fraction was added
579 to magnetic anti-Myc beads (5 µl slurry per sample; Thermofischer, 88842) and incubated for
580 2 hours at 4 °C rotating. Cells equivalent to 50 % of a 15 cm dish were used per sample. Beads
581 were washed three times in lysis buffer with 5 min incubation each, and finally boiled in 50 µl
582 Laemmli buffer (10% SDS, 200 mM Tris-HCL pH 6.0, 20% glycerol, 2.16 M β-mercaptoethanol,
583 0.01% bromphenolblue).
584
585 **Pulldown of recombinant TopBP1 fragments by immobilised GINS**
586 For in vitro pulldown experiments using recombinant GINS and TopBP1, magnetic anti-Flag
587 beads (1 µl slurry for western blot/silver staining-scale experiments, 4 µl for Coomassie-scale
588 experiments) were coupled with 600 ng (western/silver-scale) or 2400 ng (coomassie-scale)
589 GINS via 3xFlag-Sld5. 100 nM final concentration of TopBP1-Strep-WT or mutants in 20 l
590 (western/silver-scale) or 80 ul (coomassie-scale) of interaction buffer (20 mM HEPES pH8.0,

591 150mM NaCl, 0.01% (v/v) Tween-20, 0.5mM TCEP, 2% (v/v) glycerol) were added to GINS-
592 coupled beads in 5 ul (western/silver-scale) or 20 µl (coomassie-scale) interaction buffer. The
593 reaction was incubated for 45 min at 4°C rotating. Then, beads were washed three times for
594 5 min with interaction buffer and boiled in 50 µl Laemmli buffer (10% SDS, 200 mM Tris-HCL
595 pH 6.0, 20% glycerol, 2.16 M β-mercaptoethanol,0.01% bromphenolblue) before SDS PAGE.
596
597 **Pulldown from cell lysates with recombinant TopBP1-BRCT0-5-strep**
598 For pulldown assays from soluble lysates non-transfected 293T cells, 5 µl streptactin
599 Sepharose HP (Cytiva, 28935599) beads were coupled with 10 µg recombinant TopBP1-1-766-
600 strep-WT or different mutants in coupling buffer (20 mM HEPES pH8.0, 150mM NaCl, 0.1%
601 (v/v) Tween-20, 0.5mM TCEP, 2% (v/v) glycerol) for 45 min at 4 °C before washing two times
602 with coupling buffer and then once in cell lysis buffer (20 mM HEPES pH8.0, 150mM NaCl,
603 0.1% (v/v) Tween-20, 0.5mM TCEP, 2% (v/v) glycerol, protease inhibitor cocktail (Roche
604 Complete protease inhibitor cocktail, 05056489001). 293T cells were lysed in ten times pellet
605 volume of cell lysis buffer, and centrifuged at 20000 g for 15 min at 4 °C. Soluble lysate from
606 cells equivalent to 50 % of a 15 cm tissue culture plate was added to the TopBP1-coupled
607 beads and incubated for 2 h at 4°C rotating. Beads were washed three times with 5 min
608 incubation in lysis buffer and boiled in 50 µl Laemmli buffer (10% SDS, 200 mM Tris-HCL pH
609 6.0, 20% glycerol, 2.16 M β-mercaptoethanol,0.01% bromphenolblue) before SDS PAGE.
610
611 **Generation of replicating *Xenopus* egg extracts**
612 *Xenopus laevis* egg extracts were prepared from metaphase II arrested eggs as described in
613 [70]. After washing with MMR (100 mM NaCl, 2 mM KCl, 1 mM MgCl2, 2 mM CaCl2, 0.1 mM
614 EDTA, 5 mM HEPES–NaOH, pH 7.8) eggs were dejellied (2% cysteine w:v in H2O,pH 7.8 with
615 NaOH.). Subsequently, eggs were rinsed in XBE2 (100 mM KCl, 2 mM MgCl2, 0.1 mM CaCl2,
616 1.71 % w:v sucrose, 5 mM K-EGTA, 10 mM HEPES-KOH, pH 7.7). Eggs were transferred into
617 centrifuge tubes containing 1 ml XBE2 + 10 µg/ ml protease inhibitor (aprotinin Sigma A6279,
618 leupeptin Merck 108975, pepstatin Carl Roth 2936.1) + 100 µg/ ml cytochalasin D (Sigma
619 C8273). For packing, eggs were centrifuged for 1 min at 1400 g at 16 °C in a swingout rotor.
620 Excess buffer, activated and apoptotic eggs were removed before crushing the eggs at 16000
621 g for 10 min at 16 °C. Extract were collected with a 20 G needle and supplemented with 10
622 µg/ml cytochalasin D, 10 µg/ml protease inhibitors, 1:80 dilution of energy regenerator (1M
623 phosphocreatine K salt, 600 µg/ ml creatine phosphokinase in 10 mM HEPES–KOH pH 7.6)
624 and LFB1/50 (10% w:v sucrose, 50 mM KCl, 2 mM MgCl2, 1 mM EGTA, 2 mM DTT, 20 mM
625 K2HPO4/KH2PO4 pH 8.0, 40 mM HEPES–KOH, pH 8.0.) to 15 % v:v. Extract was cleared at
626 84000 g at 4 °C for 20 min in a swingout rotor. The cytoplasmatic layer was collected and
627 supplemented with 2 % glycerol v:v. Extract was frozen by dropping 20 µl aliqouts into liquid
628 nitrogen and stored at - 80 °C.
629
630 **Immunodepletion of TopBP1 from *Xenopus* egg extract:**

631 For XTopBP1 depletion from *Xenopus* egg extract, 0.5 µg antibody #1, #2 or IgG (rabbit) were
632 coupled per µl magnetic Protein G dynabeads (Life Technologies 10004D) for 1 h at RT. Freshly
633 thawed extracts were supplemented with 1/40 energy regenerator (1M phosphocreatine K
634 salt, 600 µg/ ml creatine phosphokinase in 10 mM HEPES–KOH pH 7.6) and 250 µg/ml
635 cycloheximide and released into interphase by adding 0.3 mM CaCl2 for 15 min at 23 °C.
636 Subsequently, extracts were depleted for 45 min on ice with 0.675 µg antibody per µl extract.
637 After depletion the extract was aliquoted, snap frozen and stored at - 80 °C for replication
638 assays and chromatin isolations.
639
640 **Replication analysis**
641 Interphase *Xenopus* egg extracts were supplemented with 5 ng sperm DNA (kindly provided
642 by the lab of O Stemmann) per µl extract and 50 nCi/µl α^{32}P-dCTP (Perkin Elmer
643 NEG513A250UC) at 23°C. 1 µl extract was spotted for each time point onto a glass fibre
644 membrane. For addback experiments, 6 ng/ µl recombinant TopBP1 protein or buffer was
645 added before sperm nuclei addition to TopBP1 depleted egg extract. Unbound α^{32}P-dCTP
646 was removed by rinsing the membrane three times 15 min with ice cold 5 % TCA in water
647 and once with ice cold EtOH. Newly synthesized DNA was detected by phospho-imaging.
648
649 **Chromatin isolation**
650 For chromatin isolation, XTopBP1 depleted interphase egg extract was supplemented with 50
651 µg/ml aphidicolin and aliquoted into 15 µl samples before addition of buffer or recombinant
652 TopBP1 to a final concentration 6 ng/µl. 2.25 µM geminin or buffer were added before
653 incubation for 10 min on ice. To start the replication reaction 9 ng sperm DNA/µl (I think this
654 is sperm DNA, not 9ng sperm) extract was added and incubated for 75 min at 23°C. Reactions
655 were stopped with 300 µl ice cold ELB salt (10 mM HEPES-KOH pH 7.7, 50 mM KCl, 2.5 mM
656 MgCl2) + 250 mM sucrose + 0.6 % triton X-100. Diluted extract was loaded onto 150 µl ELB
657 salt + 25 % sucrose and centrifuged for 10 min at 2500 g at 4 °C in a swingout rotor. Liquid
658 above the sucrose cushion was removed and the surface of the cushion was washed twice
659 with 200 µl EBL salt containing 250 mM sucrose. Subsequently the cushion was removed
660 leaving about 15 µl behind and centrifuged for 2 min at 10000 g at 4 °C in a fixed angle rotor
661 to remove rest of the cushionFor western blotting, the chromatin pellet was resuspended in
662 24 µl 1x Laemmli SDS sample buffer (6.5 % glycerol, 715 mM β-mercaptoethanol, 3% SDS,
663 62.5 mM Tris-HCl pH 7.9, 0.005 % Bromphenol blue) and 5 µl were separated by denaturing
664 SDS PAGE. (for anti-XCdc45 and anti-XSld5 samples were diluted again 1:5 before loading. For
665 MS analysis, chromatin pellets were analysed by CHROMASS [37]. In brief, chromatin pellets
666 were resuspended in 50 µl denaturing buffer (8 M Urea; 100 mM Tris pH 8). To reduce
667 proteins, dithiothreitol (DTT, 5 mM final concentration) was added and samples were
668 incubated at 22 °C for 30 minutes. To alkylate peptides, iodoacetamide (20 mM final) was
669 added and samples were incubated at 37 °C for 30 minutes. Finally, DTT (25 mM final) was
670 added, and samples were incubated at 22 °C for 5 minutes. To digest proteins, 500 ng Lys-C

671 (add Supplier) was added, and samples were incubated at 37 °C for 3 hours. Subsequently,
672 samples were diluted with dilution buffer (100 mM ammonium bicarbonate) to adjust the
673 urea concentration to 1 M. Trypsin (Sigma, 500 ng per sample) was added and samples were
674 incubated over night at 37 °C. Digested peptides were acidified with trifluoroacetic acid (TFA,
675 final conc. 1%)] and desalted on Empore C18 material according to Rappsilber et al.
676 *https://www.nature.com/articles/nprot.2007.261).* Eluted peptides were dried in a vacuum
677 concentrator and reconstituted with 9 µL of buffer A (0.1% formic acid) containing 0.2%
678 acetonitrile and 0.01% trifluoro acetic acid. For MS analysis, 4 µl of the reconstituted peptides
679 were separated on an EASY-nLC™ 1200 chromatography system (Thermo Scientific) coupled
680 to a Q Exactive HF-X Orbitrap LC-MS/MS System (Thermo Fisher Scientific) via a Nanoflex ion
681 source. Peptide separation was carried out in analytical columns (50 cm, 75 µm inner
682 diameter packed in-house with C18 resin ReproSilPur 120, 1.9 µm diameter Dr. Maisch) using
683 a 3-hour non-linear gradient at a flow rate of 250 nl/minute using buffer A (aqueous 0.1%
684 formic acid) and buffer B (80 % acetonitrile, 0.1% formic acid). MS data was acquired in data-
685 dependent fashion using a Top15 method. The exact parameters for chromatography and MS
686 instrument settings can be retrieved from the raw files available at ProteomeXchange (PDX-
687 XXX).
688
689 MS data files from single-shot experiments were processed with MaxQuant (version 2.0.1.0)
690 using a non-redundant *Xenopus laevis* data base available at ProteomExchange (PDX-XX) [37].
691 Raw data were normalized using the label-free quantitation (LFQ) algorithm implemented in
692 MaxQuant. MS Data with Perseus (version 1.6.15.0) [71]. Protein groups were filtered to
693 eliminate contaminants, reverse hits, and proteins identified by site only. For the heat map
694 (Fig. 5a) LFQ intensities were log2 transformed and for each protein z-scores were calculated
695 across all replicates (N=4) of all four conditions. Subsequently, the average of the z-scores
696 was calculated for each condition and selected proteins were plotted. Proteins were manually
697 annotated and sorted according to their function in DNA replication and DNA repair. To
698 identify proteins with significant abundance changes between the four conditions, LFQ
699 intensities were log2 transformed and missing values were imputed with random values
700 drawn from a normal distribution centred around the detection limit of the MS instrument
701 (Perseus imputation; width=0.3, down shift = 1.8). Two sample Student's t-tests with
702 permutation-based FDR control were carried out in Perseus. For these tests three valid values
703 in at least one quadruplicate of either of the tested conditions was required. FDR was adjusted
704 for multiple testing by the Benjamini-Hochberg procedure using a significance threshold of
705 FDR<0.05. Data visualisation was carried out in R. All scripts are available upon request.
706
707 **APEX2 biotinylation and denaturing enrichment**
708 Proximity labelling was performed in isogenic stable 293 Flip-In (Thermo Fisher; R75007) cells
709 stably expressing TopBP1 N-terminal tagged with APEX2 or in 293T cells transiently expressing
710 either N-terminal or C-terminally APEX2-tagged TopBP1. 24 h before transfection 0.8 x 10^6
711 cells were seeded onto a 6 cm plate. For each condition four dishes were used. The day after

712 transfection 90 % confluent cells were incubated for 30 min with 500 µM biotin phenol at 37
713 °C. Subsequently, cells were incubated for 1 min at RT with or without 1 mM H_2O_2. To stop
714 the biotinylation reaction, medium was discarded, and cells were washed three times with
715 quenching buffer (10 mM sodium azide, 10 mM sodium ascorbate and 5 mM Trolox in
716 Dulbecco's PBS (Life Technologies 14190169). Cells were washed off the dishes with DPBS and
717 harvest into reaction tubes and washed again with DPBS. Next, cells were lysed at 95 °C for
718 10 min in TSD buffer (50 mM Tris pH 7.5, 5 mM DTT and 1 % SDS). Samples were diluted ten
719 times with TNN buffer (20 mM Tris pH 7.9, 200 mM NaCl and 0.5 % NP-40 alternative) and
720 benzonase (75 U per sample) (Sigma E1014). Samples were incubated for 15 min at 4 °C and
721 centrifuged at 21000 g for 2 min at 4 °C. Supernatant was incubated over night with 15 µl
722 streptavidin sepharose beads (Sigma GE17-5113-01) per sample at 4 °C. After incubation
723 beads were washed once with TNN buffer + 0.1% SDS and twice with 25 mM ammonium
724 bicarbonate and then processed for mass spectrometry.
725
726 **Sample preparation of APEX2-biotiylated proteins for mass spectrometry**
727 Biotinylated proteins from PDB experiments were enriched on 15 µL streptavidin sepharose
728 beads. Captured proteins were washed 2× with H_2O prior to on-bead digestion to remove MS
729 incompatible buffer components. The beads were taken up in 100 µl 0.8 M Urea, 50 mM
730 ammonium bicarbonate buffer (ABC) and supplemented with 5 mM Dithiothreito (DTT). After
731 incubation at 37°C for 30 min, 10mM Iodoacetamide (IAM) was added and incubated for
732 another 30 min at room temperature in the dark while shaking at 1500 rpm (Thermomixer C,
733 Eppendorf). In order to quench unreacted IAM the DTT concentration was raised to a final of
734 11 mM. Trypsin digestion was initiated by adding a total of 300 ng Trypsin to each sample and
735 placing the samples at 37°C while shaking at 1150 rpm over night. The tryptic digestion was
736 stopped the next day by adding a final of 1% (vol/vol) formic acid (FA) to the samples. The
737 beads were collected by centrifugation (650× g, 5 min) and 100 µl of the supernatant
738 transferred to a Eppendorf Lo-bind 1.5 mL tube. The remaining beads were incubated with
739 50 µl 1 % formic acid for (1150 rpm, 5 min rpm, RT) and after collecting the beads once more
740 by centrifugation (650× g, 5 min) the supernatant was combined with the first one. The
741 sepharose beads were discarded. In order to remove residual sepharose beads, the combined
742 peptide containing solutions were passed over pre-equilibrated (50 µl 0.5 % formic acid)
743 home-made 2-disc Glass microfiber StageTip (disc material: GE Healthcare; pore size: 1.2 µM;
744 thickness: 0.26 mm; 50× g 2 min). The cleared tryptic digests were then desalted on home-
745 made C18 StageTips as described [72] Briefly, peptides were immobilized and washed on a 2
746 disc C18 (Empore) StageTip. After elution from the StageTips, samples were dried using a
747 vacuum concentrator (Eppendorf) and the peptides were taken up in 0.1% formic acid
748 solution (10-15 µL) and directly used for LC-MS/MS experiments (see below for details).
749
750 **BS3 crosslinking of TopBP1-BRCT0-5 and GINS**
751 50 µg (1.15 µg/µl) of each GINS and TopBP1-BRCT0-5-strep (amino acids 1-766) were
752 incubated for 45 min on ice in cross-linking buffer (20mM HEPES pH8.0, 150mM NaCl, 0.01%

753 Tween20, 2% Glycerol, 0.5mM TCEP). 600 µM or 2500 µM of BS3 crosslinker were added and
754 incubated for 30 min at 35°C with shaking. The reaction was stopped by adding ammonium
755 bicarbonate to a final concentration of 100 mM. 90 % of the cross-linked sample was used for
756 mass spectrometry analysis of crosslinks. For mass spectrometry of gel-extracted samples,
757 10% of the reaction were separated by SDS-PAGE. The coomassie-stained gel was cut in slices
758 above the molecular weight of monomeric TopBP1-BRCT0-5-strep for subsequent mass
759 spectrometry.
760
761 **Processing of BS3 crosslinked protein preparations for mass spectrometry**
762 Sample preparation of crosslinked samples for LC/MS/MS is essentially based on the SP3
763 protocol published by [73]. A volume corresponding to 30 µg of protein from each cross-linking
764 sample was taken up in 100 µL 1× SP3 Lysis Buffer (final concentrations: 5% (wt/vol) SDS; 10
765 mM TCEP; 200 µL 40 mM Chloracetamide; 200 mM HEPES pH 8) and heated for 5 min at 90°C.
766 After cooling the samples to room temperature (on ice) a mix of 150 µg hydrophobic
767 (#65152105050250) and 150 µg hydrophilic (#45152105050250) SeraMag Speed Beads
768 (Cytiva) was added to the denatured and alkylated protein containing solution (bead to
769 protein ratio 10 to 1) and gently mixed. Then 1 volume of 100% vol/vol Ethanol (EtOH) was
770 added and the protein/bead/EtOH suspension was then incubated for 20 min at 24°C on a
771 Thermomixer C (Eppendorf) while shaking at 1200 rpm. After this binding step, the beads
772 collected on a magnet washed 4× with 80% EtOH (collection time on the magnet minimum of
773 4 min). After the final wash & collect step the beads were taken up in 25 mM
774 Ammoniumbicarbonate (ABC) containing 1 µg Trypsin (Protein:Trypsin ratio 30:1). To help
775 bead dissociation samples were incubated for 5 min in a sonification bath (preheated to 37°C).
776 After this step samples were transferred to a Thermomixer C (preheated to 37°C) and
777 incubated over night while shaking at 1300 rpm. Next morning the samples were acidified
778 with formic acid (FA, final 1% vol/vol). The beads were collected on a magnet and the
779 supernatant transferred to a fresh Eppendorf tube. The samples were then put again on a
780 magnet for at least 5 min to remove remaining beads. The cleared tryptic digests were then
781 desalted on home-made C18 StageTips as described [72]. Briefly, peptides were immobilized
782 and washed on a 2 disc C18 StageTip. After elution from the StageTips, samples were dried
783 using a vacuum concentrator (Eppendorf) and the peptides were taken up in 0.1% formic acid
784 solution (10 µL) and directly used for LC-MS/MS experiments (see below for details).
785
786 **LC-MS/MS settings crosslinking mass spectrometry**
787 MS Experiments were performed on an Orbitrap Fusion LUMOS instrument (Thermo) coupled
788 to an EASY-nLC 1200 ultra-performance liquid chromatography (UPLC) system (Thermo). The
789 UPLC was operated in the one-column mode. The analytical column was a fused silica capillary
790 (75 µm × 41 cm) with an integrated fritted emitter (CoAnn Technologies) packed in-house
791 with Kinetex 1.7 µm C18-XB core shell beads (Phenomenex). The analytical column was
792 encased by a column oven (Sonation PRSO-V2) and attached to a nanospray flex ion source
793 (Thermo). The column oven temperature was set to 50 °C during sample loading and data

794 acquisition. The LC was equipped with two mobile phases: solvent A (0.2% FA, 2% Acetonitrile,
795 ACN, 97.8% H_2O) and solvent B (0.2% FA, 80% ACN, 19.8% H_2O). All solvents were of UPLC
796 grade (Honeywell). Peptides were directly loaded onto the analytical column with a maximum
797 flow rate that would not exceed the set pressure limit of 980 bar (usually around 0.4 – 0.6
798 µL/min). Peptides were subsequently separated on the analytical column by running a 70 min
799 gradient of solvent A and solvent B (start with 2% B; gradient 2% to 6% B for 5:00 min; gradient
800 6% to 25% B for 42:00 min; gradient 25% to 40% B for 15:00 min; 40% to 98% B for 1:00 min;
801 98% for 7:00 min) at a flow rate of 350 nl/min. The mass spectrometer was controlled by the
802 Orbitrap Fusion Lumos Tune Application (version 3.3.2782.28) and operated using the
803 Xcalibur software (version 4.3.73.11). The mass spectrometer was set in the positive ion
804 mode. The ionization potential (spray voltage) was set to 2.5 kV. Source fragmentation was
805 turned off. Precursor ion scanning was performed in the Orbitrap analyser (FT; fourier
806 transform mass spectrometer) in the scan range of m/z 370-1600 and at a resolution of
807 120000 with the internal lock mass option turned on (lock mass was 445.120025 m/z,
808 polysiloxane) [74]. AGC (automatic gain control) was set to "standard" and acquisition time to
809 "auto". Product ion spectra were recorded in a data dependent fashion in the FT in a variable
810 scan range ("auto") and at 15000 resolution. Peptides were analysed using a "top speed"
811 regime (repeating cycle of full precursor ion scan (AGC target "standard"; acquisition time
812 "200ms") followed by dependent MS2 scans for 5 seconds (minimum intensity threshold
813 2×10^4). The MS2 precursor ions were isolated using the quadrupole (isolation window 2.0
814 m/z) and fragmentation was achieved by Higher-energy C-trap dissociation (HCD) (normalized
815 collision mode set to "stepped" and normalized collision energy set to "27, 30, 33%"). During
816 MS2 data acquisition dynamic ion exclusion was set to 60 seconds. Only charge states
817 between 3-7 were considered for fragmentation.
818
819 **LC-MS/MS settings for PDB experiments**
820 MS Experiments were performed on an Orbitrap Fusion LUMOS instrument (Thermo) coupled
821 to an EASY-nLC 1200 ultra-performance liquid chromatography (UPLC) system (Thermo). The
822 UPLC was operated in the one-column mode. The analytical column was a fused silica capillary
823 (75 µm × 46 cm) with an integrated fritted emitter (CoAnn Technologies) packed in-house
824 with Kinetex 1.7 µm C18-XB core shell beads (Phenomenex). The analytical column was
825 encased by a column oven (Sonation PRSO-V2) and attached to a nanospray flex ion source
826 (Thermo). The column oven temperature was set to 50 °C during sample loading and data
827 acquisition. The LC was equipped with two mobile phases: solvent A (0.2% FA, 2% Acetonitrile,
828 ACN, 97.8% H_2O) and solvent B (0.2% FA, 80% ACN, 19.8% H_2O). All solvents were of UPLC
829 grade (Honeywell). Peptides were directly loaded onto the analytical column with a maximum
830 flow rate that would not exceed the set pressure limit of 980 bar (usually around 0.4 – 0.6
831 µL/min). Peptides were subsequently separated on the analytical column by running a 105
832 min gradient of solvent A and solvent B (start with 3% B; gradient 3% to 9% B for 6:30 min;
833 gradient 9% to 30% B for 62:30 min; gradient 30% to 50% B for 24:00 min; 50% to 100% B for
834 2:30 min; 100% for 9:30 min) at a flow rate of 300 nl/min. The mass spectrometer was

835 controlled by the Orbitrap Fusion Lumos Tune Application (version 3.3.2782.28) and operated
836 using the Xcalibur software (version 4.3.73.11). The mass spectrometer was set in the positive
837 ion mode. The ionization potential (spray voltage) was set to 2.5 kV. Source fragmentation
838 was turned off. Precursor ion scanning was performed in the Orbitrap analyser (FT; fourier
839 transform mass spectrometer) in the scan range of m/z 370-1500 and at a resolution of
840 240000 with the internal lock mass option turned on (lock mass was 445.120025 m/z,
841 polysiloxane) [74]. AGC (automatic gain control) was set to "standard" and acquisition time to
842 "auto". Product ion spectra were recorded in a data dependent fashion in the IT (IT; ion trap
843 mass spectrometer) in a variable scan range ("auto") and at "rapid" scan rate. Peptides were
844 analysed using a "top speed" regime (repeating cycle of full precursor ion scan (AGC target
845 "300%"; acquisition time "auto") followed by dependent MS2 scans for 3 seconds (minimum
846 intensity threshold 4×10^3)). The MS2 precursor ions were isolated using the quadrupole
847 (isolation window 1.6 m/z) and fragmentation was achieved by Higher-energy C-trap
848 dissociation (HCD) (normalized collision mode set to "stepped" and normalized collision
849 energy set to "27, 32, 40%"). During MS2 data acquisition dynamic ion exclusion was set to
850 20 seconds. Only charge states between 2-7 were considered for fragmentation.
851
852 **Data processing protocol on-bead digestion**
853 RAW spectra were submitted to an Andromeda [75] search in MaxQuant (v2.0.3.0) using the
854 default settings (Cox & Mann 2008) [76]. Label-free quantification and match-between-runs was
855 activated [77]. The MS/MS spectra data were searched against the Uniprot *H. sapiens* reference
856 database (one protein per gene; UP000005640_9606_OPPG.fasta, 20585 entries,
857 downloaded 1/10/2022) and a dedicated database containing the APEX2-myc sequence
858 (ACE_0741_SOI_v01.fasta; 1 entry). All searches included a contaminants database search (as
859 implemented in MaxQuant, 246 entries). The contaminants database contains known MS
860 contaminants and was included to estimate the level of contamination. Andromeda searches
861 allowed oxidation of methionine residues (16 Da) and acetylation of the protein N-terminus
862 (42 Da) as dynamic modifications and the static modification of cysteine (57 Da, alkylation
863 with iodoacetamide). Enzyme specificity was set to "Trypsin/P" with two missed cleavages
864 allowed. The instrument type in Andromeda searches was set to Orbitrap and the precursor
865 mass tolerance was set to ± 20 ppm (first search) and ± 4.5 ppm (main search). The MS/MS
866 match tolerance was set to ± 0.5 Da. The peptide spectrum match FDR and the protein FDR
867 were set to 0.01 (based on target-decoy approach). Minimum peptide length was 7 aa. For
868 protein quantification unique and razor peptides were allowed. Modified peptides were
869 allowed for quantification. The minimum score for modified peptides was 40. Label-free
870 protein quantification was switched on, and unique and razor peptides were considered for
871 quantification with a minimum ratio count of 2. Retention times were recalibrated based on
872 the built-in nonlinear time-rescaling algorithm. MS/MS identifications were transferred
873 between LC-MS/MS runs with the "match between runs" option in which the maximal match
874 time window was set to 0.7 min and the alignment time window set to 20 min. The
875 quantification is based on the "value at maximum" of the extracted ion current. At least two

876 quantitation events were required for a quantifiable protein. Further analysis and filtering of
877 the results was done in Perseus v1.6.10.0. [71]. For quantification we combined related
878 biological replicates to categorical groups and investigated only those proteins that were
879 found in at least one categorical group in a minimum of 3 out of 4 biological replicates.
880 Comparison of protein group quantities (relative quantification) between different MS runs
881 is based solely on the LFQ's as calculated by MaxQuant, MaxLFQ algorithm [77].
882
883 **Data processing protocol for crosslinking experiments**
884 The searches for crosslinked peptides were performed with two different search engines:
885 MetaMorpheus (MM) version 0.0.320 [78] and pLink2 version v2.3.9. [79]. Searches were
886 performed on the Thermo RAW files using the database ACE_0704_SOI_plus_con_v01.fasta
887 (244 entries). The database contains the sequences for TopBP1 (1-766), PsfI, PsFII, PsfIII, Sld5
888 and 239 known contaminating proteins found in MS samples. The peptide spectrum match
889 FDR for MM was 0.01 and for pLink2 0.05 (based on target-decoy approach, decoys are
890 generated by the software). The settings for MetaMorpheus were: crosslinker name = DSS
891 _KSTY (note: DSS and BS3 have identical crosslinker size); crosslinker type = non-cleavable;
892 crosslinker mass = 138.06808; crosslinker modification site 1 = K; crosslinker modification site
893 2 = KSTY; protease = trypsin; maximum missed cleavages = 3; minimum peptide length = 5;
894 maximum peptide length = 60; initiator methionine behaviour = Variable; max modification
895 isoforms = 1024; fixed modifications = Carbamidomethyl on C, variable modifications =
896 Oxidation on M; parent mass tolerance(s) = ±10 ppm; product mass tolerance = ±20 ppm. The
897 settings for pLink2 were: crosslinker name = DSS-BS3-KSTY; crosslinker type = non-cleavable;
898 crosslinker mass = 138.06808; crosslinker modification site 1 = K; crosslinker modification site
899 2 = KSTY; protease = trypsin; maximum missed cleavages = 3; minimum peptide length = 6;
900 maximum peptide length = 60; fixed modifications = Carbamidomethyl on C, variable
901 modifications = Oxidation on M; parent mass tolerance(s) = ±20 ppm; product mass tolerance
902 = ±20 ppm. The results from both searches were converted to the ProXL XML format using
903 the respective converters (metaMorph2ProxlXML.jar, plink2toProxlXML.jar, follow links on
904 the ProXL website; https://proxl-ms.org/) and uploaded to the ProXL server [80]. Analysis and
905 evaluation of crosslinks was performed on our local ProXL Server. The results from both
906 searches was analysed together.
907
908 **Computational modeling**
909 We used the local implementation of AlphaFold-Multime (deepmind.com) to predict the
910 binding interfaces of GINS and TopBP1 using the full-length sequence of each chain. 25
911 models were obtained by default and ranked with the combined score of ipTM+pTM
912 implemented in AlphaFold-Multimer [81].
913 To gain more insights into the GINI binding region, we performed blind molecular docking
914 calculations taking the GINI sequence DEDLLSQY of TopBP1 (residues 487-494) with Cluspro
915 [82], HPEPDOCK [83], and MDockPeP [84] web servers, for 200 solutions per server. We further
916 extended, refined, and re-scored the sampling, by generating 10 additional conformations

917 per web server solution (for a total of 6000 solutions) with FlexPepDock [85]. The top-10 best-
918 scored solutions were selected for analysis and visualization.
919 The binding free energies of GINS with BRCT45 and GINI were estimated with the PRODIGY [86]
920 and PPI-Affinity [87] web servers. For the estimations, the best scored AlphaFold model was
921 used. The region of GINI employed for the estimation of the binding free energies comprised
922 residues 481 to 496.
923
924 **Grid preparation**
925 Quantifoil 1.2/1.3, 300 mesh copper grids (Quantifoil) were glow discharged using a Tergeo
926 Plasma Cleaner (Pie Scientific) with an indirect plasma treatment for 30 seconds. Grids were
927 loaded into a Leica EM GP2 (Leica microsystems) and 3 µl of peak fractions from size exclusion
928 chromatography were diluted to 0.1 mg/ml and applied to the front of the grid, with an
929 additional 0.5 µl buffer applied to the grids rear, before back blotting for 3 seconds and
930 plunging into an ethane propane mix.
931
932 **Grid preparation**
933 Quantifoil 1.2/1.3, 300 mesh copper grids (Quantifoil) were glow discharged using a Tergeo
934 Plasma Cleaner (Pie Scientific) with an indirect plasma treatment for 30 seconds. Grids were
935 loaded into a Leica EM GP2 (Leica microsystems) and 3 µl of peak fractions from size exclusion
936 chromatography were diluted to 0.1 mg/ml and applied to the front of the grid, with an
937 additional 0.5 µl buffer applied to the grids rear, before back blotting for 3 seconds and
938 plunging into an ethane propane mix.
939
940 **Electron microscopy and data processing - Dataset one**
941 Grids were stored in liquid nitrogen prior to imaging at 300 kV on a FEI Titan Krios (Thermo
942 Fisher Scientific) equipped with K3 detector (Gatan). 18945 movies were collected, using data
943 acquisition software EPU (Thermo Fisher Scientific), at a magnification of 105000 and a pixel
944 size of 0.85Å using a total dose of 50 e-/Å2. These were motion corrected in 5x5 patches using
945 MOTIONCORE2 implemented in RELION4.0 before importing into cryoSPARC. Micrographs
946 were CTF corrected prior to blob picking and extraction of an initial set of particles.
947 Subsequent filtering by 2D classification removed most of these leaving a cleaned set of
948 particles that were used to produce 4 initial models. The 2D classes and initial models
949 appeared to have at least two distinct sub populations, one containing just the GINS complex
950 alone and one that also had some additional density. In order to distinguish between these
951 two sets of particles heterorefinement was performed to split the two groups. The first
952 population of particles containing only the GINS complex were then imported into RELION4.0
953 before several cycles of 3D classification, to yield a final set of 111455 particles that gave a
954 volume at 5.9 Å resolution used to produce the GINS alone volume used in Fig. 6-S1a. The
955 second group of TOPBP1-GINS particles were used to train a TOPAZ model before
956 implementing further picking using TOPAZ. The resulting particles were again filtered by
957 rounds of 2D classification and heterorefinement before exporting the particles, that

appeared to consist of the full TOPBP1-GINS complex, into RELION4.0. Several cycles of 3D classification were then performed with classes appearing to lack the additional density eliminated, to yield a final set of 208115 particles. 3D refinement and post-processing of these gave a volume at 4.71Å resolution into which previously solved crystal structures of the GINS complex (29EX) and the central BRCT4/5 module of TopBP1 (3UEN) could be docked.

Electron microscopy and data processing - Dataset two

Grids were stored in liquid nitrogen prior to imaging at 300 kV on a FEI Titan Krios (Thermo Fisher Scientific) equipped with Fakcon 4i detector (Thermo Fisher Scientific). 8808 movies were collected, using data acquisition software EPU (Thermo Fisher Scientific), at a magnification of 120000 and a pixel size of 0.74Å using a total dose of 39.69 e-/Å2. The same processing schedule was followed as for dataset one to yield a final set of 154278 particles. 3D refinement and post-processing of these gave a volume at 4.1 Å resolution into which the previously solved model could be docked alongside the predicted GINI helix from the Alphafold2 model. Minor adjustments to the model were made in Coot before refinement of the final model using PHENIX.

Data Presentation

Figure panels for all structural data were produced using ChimeraX-1.3

Data Availability

The mass spectrometry proteomics data for the proximity dependent biotinylation experiments, the cross-linking experiments and the chromatin mass spectrometry (CHROMASS) experiments have been deposited to the ProteomeXchange Consortium via the PRIDE[88] partner repository (https://www.ebi.ac.uk/pride/archive/) with the dataset identifiers PXD040000 (PDB experiments), PXD040156 (CL-MS experiments) and PXD040024 (CHROMASS experiments). During the review process the data can be accessed via the following Reviewer accounts:

PXD040000: (Username: reviewer_pxd040000@ebi.ac.uk; Password: Lk9VLXVF)

PXD040156: (Username: reviewer_pxd040156@ebi.ac.uk; Password: NLNLORQl)

PXD040024: (Username: reviewer_pxd040024@ebi.ac.uk; Password: 5OGweuE6)

Cryo-EM maps and refined coordinates have been deposited in the EMDB and Protein Databank as EMD- 16916 and PDB ID 8OK2 respectively.

Competing interests

none

997 **References**

998

999 1 Costa, A. & Diffley, J. F. X. The Initiation of Eukaryotic DNA Replication. *Annu Rev*
1000 *Biochem* **91**, 107-131 (2022). https://doi.org:10.1146/annurev-biochem-072321-
1001 110228
1002 2 Siddiqui, K., On, K. F. & Diffley, J. F. Regulating DNA replication in eukarya. *Cold Spring*
1003 *Harb Perspect Biol* **5** (2013). https://doi.org:10.1101/cshperspect.a012930
1004 3 Remus, D. *et al.* Concerted loading of Mcm2-7 double hexamers around DNA during
1005 DNA replication origin licensing. *Cell* **139**, 719-730 (2009). https://doi.org:S0092-
1006 8674(09)01303-8 [pii]
1007 10.1016/j.cell.2009.10.015
1008 4 Evrin, C. *et al.* A double-hexameric MCM2-7 complex is loaded onto origin DNA during
1009 licensing of eukaryotic DNA replication. *Proc Natl Acad Sci U S A* **106**, 20240-20245
1010 (2009). https://doi.org:0911500106 [pii]
1011 10.1073/pnas.0911500106
1012 5 Georgescu, R. *et al.* Structure of eukaryotic CMG helicase at a replication fork and
1013 implications to replisome architecture and origin initiation. *Proc Natl Acad Sci U S A*
1014 **114**, E697-E706 (2017). https://doi.org:10.1073/pnas.1620500114
1015 6 Douglas, M. E., Ali, F. A., Costa, A. & Diffley, J. F. X. The mechanism of eukaryotic CMG
1016 helicase activation. *Nature* **555**, 265-268 (2018).
1017 https://doi.org:10.1038/nature25787
1018 7 Moyer, S. E., Lewis, P. W. & Botchan, M. R. Isolation of the Cdc45/Mcm2-7/GINS (CMG)
1019 complex, a candidate for the eukaryotic DNA replication fork helicase. *Proc Natl Acad*
1020 *Sci U S A* **103**, 10236-10241 (2006).
1021 8 Ilves, I., Petojevic, T., Pesavento, J. J. & Botchan, M. R. Activation of the MCM2-7
1022 helicase by association with Cdc45 and GINS proteins. *Mol Cell* **37**, 247-258 (2010).
1023 https://doi.org:S1097-2765(09)00963-0 [pii]
1024 10.1016/j.molcel.2009.12.030
1025 9 Costa, A. *et al.* DNA binding polarity, dimerization, and ATPase ring remodeling in the
1026 CMG helicase of the eukaryotic replisome. *Elife* **3**, e03273 (2014).
1027 https://doi.org:10.7554/eLife.03273
1028 10 Yeeles, J. T., Deegan, T. D., Janska, A., Early, A. & Diffley, J. F. Regulated eukaryotic
1029 DNA replication origin firing with purified proteins. *Nature* **519**, 431-435 (2015).
1030 https://doi.org:10.1038/nature14285
1031 11 Lewis, J. S. *et al.* Mechanism of replication origin melting nucleated by CMG helicase
1032 assembly. *Nature* **606**, 1007-1014 (2022). https://doi.org:10.1038/s41586-022-
1033 04829-4
1034 12 Kanemaki, M. & Labib, K. Distinct roles for Sld3 and GINS during establishment and
1035 progression of eukaryotic DNA replication forks. *Embo J* **25**, 1753-1763 (2006).
1036 13 Heller, R. C. *et al.* Eukaryotic Origin-Dependent DNA Replication In Vitro Reveals
1037 Sequential Action of DDK and S-CDK Kinases. *Cell* **146**, 80-91 (2011).
1038 https://doi.org:S0092-8674(11)00654-4 [pii]
1039 10.1016/j.cell.2011.06.012
1040 14 Francis, L. I., Randell, J. C., Takara, T. J., Uchima, L. & Bell, S. P. Incorporation into the
1041 prereplicative complex activates the Mcm2-7 helicase for Cdc7-Dbf4 phosphorylation.
1042 *Genes Dev* **23**, 643-654 (2009).

1043 15 Greiwe, J. F. *et al.* Structural mechanism for the selective phosphorylation of DNA-
1044 loaded MCM double hexamers by the Dbf4-dependent kinase. *Nat Struct Mol Biol* **29**,
1045 10-20 (2022). https://doi.org:10.1038/s41594-021-00698-z
1046 16 Saleh, A. *et al.* The structural basis of Cdc7-Dbf4 kinase dependent targeting and
1047 phosphorylation of the MCM2-7 double hexamer. *Nat Commun* **13**, 2915 (2022).
1048 https://doi.org:10.1038/s41467-022-30576-1
1049 17 Itou, H., Muramatsu, S., Shirakihara, Y. & Araki, H. Crystal structure of the homology
1050 domain of the eukaryotic DNA replication proteins Sld3/Treslin. *Structure* **22**, 1341-
1051 1347 (2014). https://doi.org:10.1016/j.str.2014.07.001
1052 18 Zegerman, P. & Diffley, J. F. X. Phosphorylation of Sld2 and Sld3 by cyclin-dependent
1053 kinases promotes DNA replication in budding yeast. *Nature* **445**, 281-285 (2007).
1054 https://doi.org:nature05432 [pii]
1055 10.1038/nature05432
1056 19 Kumagai, A., Shevchenko, A. & Dunphy, W. G. Direct regulation of Treslin by cyclin-
1057 dependent kinase is essential for the onset of DNA replication. *J Cell Biol* **193**, 995-
1058 1007 (2011). https://doi.org:jcb.201102003 [pii]
1059 10.1083/jcb.201102003
1060 20 Boos, D. *et al.* Regulation of DNA Replication through Sld3-Dpb11 Interaction Is
1061 Conserved from Yeast to Humans. *Curr Biol* **21**, 1152-1157 (2011).
1062 https://doi.org:S0960-9822(11)00644-0 [pii]
1063 10.1016/j.cub.2011.05.057
1064 21 Tak, Y. S., Tanaka, Y., Endo, S., Kamimura, Y. & Araki, H. A CDK-catalysed regulatory
1065 phosphorylation for formation of the DNA replication complex Sld2-Dpb11. *Embo J* **25**,
1066 1987-1996 (2006).
1067 22 Gambus, A. *et al.* GINS maintains association of Cdc45 with MCM in replisome
1068 progression complexes at eukaryotic DNA replication forks. *Nat Cell Biol* **8**, 358-366
1069 (2006). https://doi.org:ncb1382 [pii]
1070 10.1038/ncb1382
1071 23 Sengupta, S., van Deursen, F., de Piccoli, G. & Labib, K. Dpb2 integrates the leading-
1072 strand DNA polymerase into the eukaryotic replisome. *Curr Biol* **23**, 543-552 (2013).
1073 https://doi.org:10.1016/j.cub.2013.02.011
1074 24 Goswami, P. *et al.* Structure of DNA-CMG-Pol epsilon elucidates the roles of the non-
1075 catalytic polymerase modules in the eukaryotic replisome. *Nat Commun* **9**, 5061
1076 (2018). https://doi.org:10.1038/s41467-018-07417-1
1077 25 Jones, M. L., Baris, Y., Taylor, M. R. G. & Yeeles, J. T. P. Structure of a human replisome
1078 shows the organisation and interactions of a DNA replication machine. *EMBO J* **40**,
1079 e108819 (2021). https://doi.org:10.15252/embj.2021108819
1080 26 Day, M., Oliver, A. W. & Pearl, L. H. Phosphorylation-dependent assembly of DNA
1081 damage response systems and the central roles of TOPBP1. *DNA Repair (Amst)* **108**,
1082 103232 (2021). https://doi.org:10.1016/j.dnarep.2021.103232
1083 27 Makiniemi, M. *et al.* BRCT domain-containing protein TopBP1 functions in DNA
1084 replication and damage response. *J Biol Chem* **276**, 30399-30406 (2001).
1085 28 Kumagai, A., Shevchenko, A. & Dunphy, W. G. Treslin collaborates with TopBP1 in
1086 triggering the initiation of DNA replication. *Cell* **140**, 349-359 (2010).
1087 https://doi.org:S0092-8674(09)01635-3 [pii]
1088 10.1016/j.cell.2009.12.049

1089 29 Tanaka, S. *et al.* Efficient initiation of DNA replication in eukaryotes requires
1090 Dpb11/TopBP1-GINS interaction. *Mol Cell Biol* **33**, 2614-2622 (2013).
1091 https://doi.org:10.1128/MCB.00431-13
1092 30 Mantiero, D., Mackenzie, A., Donaldson, A. & Zegerman, P. Limiting replication
1093 initiation factors execute the temporal programme of origin firing in budding yeast.
1094 *EMBO J* **30**, 4805-4814 (2011). https://doi.org:10.1038/emboj.2011.404
1095 31 Tanaka, S., Nakato, R., Katou, Y., Shirahige, K. & Araki, H. Origin association of Sld3,
1096 Sld7, and Cdc45 proteins is a key step for determination of origin-firing timing. *Curr*
1097 *Biol* **21**, 2055-2063 (2011). https://doi.org:10.1016/j.cub.2011.11.038
1098 32 Collart, C., Allen, G. E., Bradshaw, C. R., Smith, J. C. & Zegerman, P. Titration of four
1099 replication factors is essential for the Xenopus laevis midblastula transition. *Science*
1100 **341**, 893-896 (2013). https://doi.org:10.1126/science.1241530
1101 33 Bigot, N. *et al.* Phosphorylation-mediated interactions with TOPBP1 couple 53BP1 and
1102 9-1-1 to control the G1 DNA damage checkpoint. *Elife* **8** (2019).
1103 https://doi.org:10.7554/eLife.44353
1104 34 DiIorio, M. C. & Kulczyk, A. W. A Robust Single-Particle Cryo-Electron Microscopy
1105 (cryo-EM) Processing Workflow with cryoSPARC, RELION, and Scipion. *J Vis Exp* (2022).
1106 https://doi.org:10.3791/63387
1107 35 Kimanius, D., Dong, L., Sharov, G., Nakane, T. & Scheres, S. H. W. New tools for
1108 automated cryo-EM single-particle analysis in RELION-4.0. *Biochem J* **478**, 4169-4185
1109 (2021). https://doi.org:10.1042/BCJ20210708
1110 36 Leung, C. C. *et al.* Structural insights into recognition of MDC1 by TopBP1 in DNA
1111 replication checkpoint control. *Structure* **21**, 1450-1459 (2013).
1112 https://doi.org:10.1016/j.str.2013.06.015
1113 37 Raschle, M. *et al.* DNA repair. Proteomics reveals dynamic assembly of repair
1114 complexes during bypass of DNA cross-links. *Science* **348**, 1253671 (2015).
1115 https://doi.org:10.1126/science.1253671
1116 38 Kamada, K., Kubota, Y., Arata, T., Shindo, Y. & Hanaoka, F. Structure of the human
1117 GINS complex and its assembly and functional interface in replication initiation. *Nat*
1118 *Struct Mol Biol* **14**, 388-396 (2007).
1119 39 Chang, Y. P., Wang, G., Bermudez, V., Hurwitz, J. & Chen, X. S. Crystal structure of the
1120 GINS complex and functional insights into its role in DNA replication. *Proc Natl Acad*
1121 *Sci U S A* **104**, 12685-12690 (2007).
1122 40 De Jesus-Kim, L. *et al.* DDK regulates replication initiation by controlling the
1123 multiplicity of Cdc45-GINS binding to Mcm2-7. *Elife* **10** (2021).
1124 https://doi.org:10.7554/eLife.65471
1125 41 Deegan, T. D., Yeeles, J. T. & Diffley, J. F. Phosphopeptide binding by Sld3 links Dbf4-
1126 dependent kinase to MCM replicative helicase activation. *EMBO J* **35**, 961-973 (2016).
1127 https://doi.org:10.15252/embj.201593552
1128 42 Looke, M., Maloney, M. F. & Bell, S. P. Mcm10 regulates DNA replication elongation
1129 by stimulating the CMG replicative helicase. *Genes Dev* **31**, 291-305 (2017).
1130 https://doi.org:10.1101/gad.291336.116
1131 43 Douglas, M. E. & Diffley, J. F. X. Recruitment of Mcm10 to Sites of Replication Initiation
1132 Requires Direct Binding to the Minichromosome Maintenance (MCM) Complex. *J Biol*
1133 *Chem* **291**, 5879-5888 (2016). https://doi.org:10.1074/jbc.M115.707802

1134 44 Zegerman, P. & Diffley, J. F. X. Checkpoint-dependent inhibition of DNA replication
1135 initiation by Sld3 and Dbf4 phosphorylation. *Nature* **467**, 474-478 (2010).
1136 https://doi.org:nature09373 [pii]
1137 10.1038/nature09373
1138 45 Lopez-Mosqueda, J. *et al.* Damage-induced phosphorylation of Sld3 is important to
1139 block late origin firing. *Nature* **467**, 479-483 (2010). https://doi.org:nature09377 [pii]
1140 10.1038/nature09377
1141 46 Natsume, T. *et al.* Kinetochores coordinate pericentromeric cohesion and early DNA
1142 replication by Cdc7-Dbf4 kinase recruitment. *Mol Cell* **50**, 661-674 (2013).
1143 https://doi.org:10.1016/j.molcel.2013.05.011
1144 47 Reusswig, K. U., Zimmermann, F., Galanti, L. & Pfander, B. Robust Replication Control
1145 Is Generated by Temporal Gaps between Licensing and Firing Phases and Depends on
1146 Degradation of Firing Factor Sld2. *Cell Rep* **17**, 556-569 (2016).
1147 https://doi.org:10.1016/j.celrep.2016.09.013
1148 48 Tanaka, S. Interaction of replication factor Sld3 and histone acetyl transferase Esa1
1149 alleviates gene silencing and promotes the activation of late and dormant replication
1150 origins. *Genetics* **217**, 1-11 (2021). https://doi.org:10.1093/genetics/iyaa001
1151 49 Sansam, C. G. *et al.* A mechanism for epigenetic control of DNA replication. *Genes Dev*
1152 **32**, 224-229 (2018). https://doi.org:10.1101/gad.306464.117
1153 50 Wittig, K. A., Sansam, C. G., Noble, T. D., Goins, D. & Sansam, C. L. The CRL4DTL E3
1154 ligase induces degradation of the DNA replication initiation factor TICRR/TRESLIN
1155 specifically during S phase. *Nucleic Acids Res* **49**, 10507-10523 (2021).
1156 https://doi.org:10.1093/nar/gkab805
1157 51 Johnson, M. C., Can, G., Santos, M. M., Alexander, D. & Zegerman, P. Checkpoint
1158 inhibition of origin firing prevents inappropriate replication outside of S-phase. *Elife*
1159 **10** (2021). https://doi.org:10.7554/eLife.63589
1160 52 Ferreira, P. *et al.* MTBP phosphorylation controls DNA replication origin firing. *Sci Rep*
1161 **11**, 4242 (2021). https://doi.org:10.1038/s41598-021-83287-w
1162 53 Ciardo, D. *et al.* Polo-like kinase 1 (Plk1) regulates DNA replication origin firing and
1163 interacts with Rif1 in Xenopus. *Nucleic Acids Res* **49**, 9851-9869 (2021).
1164 https://doi.org:10.1093/nar/gkab756
1165 54 Bohly, N. *et al.* Increased replication origin firing links replication stress to whole
1166 chromosomal instability in human cancer. *Cell Rep* **41**, 111836 (2022).
1167 https://doi.org:10.1016/j.celrep.2022.111836
1168 55 Toledo, L. I. *et al.* ATR prohibits replication catastrophe by preventing global
1169 exhaustion of RPA. *Cell* **155**, 1088-1103 (2013).
1170 https://doi.org:10.1016/j.cell.2013.10.043
1171 56 Helmrich, A., Ballarino, M., Nudler, E. & Tora, L. Transcription-replication encounters,
1172 consequences and genomic instability. *Nat Struct Mol Biol* **20**, 412-418 (2013).
1173 https://doi.org:10.1038/nsmb.2543
1174 57 Rhind, N. & Gilbert, D. M. DNA replication timing. *Cold Spring Harb Perspect Biol* **5**,
1175 a010132 (2013). https://doi.org:10.1101/cshperspect.a010132
1176 58 Boos, D. & Ferreira, P. Origin Firing Regulations to Control Genome Replication Timing.
1177 *Genes (Basel)* **10** (2019). https://doi.org:10.3390/genes10030199
1178 59 Burrell, R. A. *et al.* Replication stress links structural and numerical cancer
1179 chromosomal instability. *Nature* **494**, 492-496 (2013).
1180 https://doi.org:10.1038/nature11935

1181 60 Volpi, I., Gillespie, P. J., Chadha, G. S. & Blow, J. J. The role of DDK and Treslin-MTBP in
1182 coordinating replication licensing and pre-initiation complex formation. *Open Biol* **11**,
1183 210121 (2021). https://doi.org:10.1098/rsob.210121
1184 61 Gaggioli, V. *et al.* CDK phosphorylation of SLD-2 is required for replication initiation
1185 and germline development in C. elegans. *J Cell Biol* **204**, 507-522 (2014).
1186 https://doi.org:10.1083/jcb.201310083
1187 62 Fukuura, M. *et al.* CDK promotes interactions of Sld3 and Drc1 with Cut5 for initiation
1188 of DNA replication in fission yeast. *Mol Biol Cell* **22**, 2620-2633 (2011).
1189 https://doi.org:mbc.E10-12-0995 [pii]
1190 10.1091/mbc.E10-12-0995
1191 63 Muramatsu, S., Hirai, K., Tak, Y. S., Kamimura, Y. & Araki, H. CDK-dependent complex
1192 formation between replication proteins Dpb11, Sld2, Pol (epsilon}, and GINS in
1193 budding yeast. *Genes Dev* **24**, 602-612 (2010). https://doi.org:24/6/602 [pii]
1194 10.1101/gad.1883410
1195 64 Rappas, M., Oliver, A. W. & Pearl, L. H. Structure and function of the Rad9-binding
1196 region of the DNA-damage checkpoint adaptor TopBP1. *Nucleic Acids Res* (2010).
1197 https://doi.org:gkq743 [pii]
1198 10.1093/nar/gkq743
1199 65 Ferreira, P., Sanchez-Pulido, L., Marko, A., Ponting, C. P. & Boos, D. Refining the
1200 domain architecture model of the replication origin firing factor Treslin/TICRR. *Life Sci*
1201 *Alliance* **5** (2022). https://doi.org:10.26508/lsa.202101088
1202 66 Chou, D. M., Petersen, P., Walter, J. C. & Walter, G. Protein phosphatase 2A regulates
1203 binding of Cdc45 to the prereplication complex. *J Biol Chem* **277**, 40520-40527 (2002).
1204 67 Kohler, K. *et al.* The Cdk8/19-cyclin C transcription regulator functions in genome
1205 replication through metazoan Sld7. *PLoS Biol* **17**, e2006767 (2019).
1206 https://doi.org:10.1371/journal.pbio.2006767
1207 68 Zimmerman, K. M., Jones, R. M., Petermann, E. & Jeggo, P. A. Diminished origin-
1208 licensing capacity specifically sensitizes tumor cells to replication stress. *Mol Cancer*
1209 *Res* **11**, 370-380 (2013). https://doi.org:10.1158/1541-7786.MCR-12-0491
1210 69 Rainey, M. D., Quachthithu, H., Gaboriau, D. & Santocanale, C. DNA Replication
1211 Dynamics and Cellular Responses to ATP Competitive CDC7 Kinase Inhibitors. *ACS*
1212 *Chem Biol* **12**, 1893-1902 (2017). https://doi.org:10.1021/acschembio.7b00117
1213 70 Gillespie, P. J., Gambus, A. & Blow, J. J. Preparation and use of Xenopus egg extracts
1214 to study DNA replication and chromatin associated proteins. *Methods* **57**, 203-213
1215 (2012). https://doi.org:10.1016/j.ymeth.2012.03.029
1216 71 Tyanova, S. *et al.* The Perseus computational platform for comprehensive analysis of
1217 (prote)omics data. *Nat Methods* **13**, 731-740 (2016).
1218 https://doi.org:10.1038/nmeth.3901
1219 72 Rappsilber, J., Mann, M. & Ishihama, Y. Protocol for micro-purification, enrichment,
1220 pre-fractionation and storage of peptides for proteomics using StageTips. *Nat Protoc*
1221 **2**, 1896-1906 (2007). https://doi.org:10.1038/nprot.2007.261
1222 73 Hughes, C. S. *et al.* Single-pot, solid-phase-enhanced sample preparation for
1223 proteomics experiments. *Nat Protoc* **14**, 68-85 (2019).
1224 https://doi.org:10.1038/s41596-018-0082-x
1225 74 Olsen, J. V. *et al.* Parts per million mass accuracy on an Orbitrap mass spectrometer
1226 via lock mass injection into a C-trap. *Mol Cell Proteomics* **4**, 2010-2021 (2005).
1227 https://doi.org:10.1074/mcp.T500030-MCP200

75 Cox, J. *et al.* Andromeda: a peptide search engine integrated into the MaxQuant environment. *J Proteome Res* **10**, 1794-1805 (2011). https://doi.org:10.1021/pr101065j
76 Cox, J. & Mann, M. MaxQuant enables high peptide identification rates, individualized p.p.b.-range mass accuracies and proteome-wide protein quantification. *Nat Biotechnol* **26**, 1367-1372 (2008). https://doi.org:10.1038/nbt.1511
77 Cox, J. *et al.* Accurate proteome-wide label-free quantification by delayed normalization and maximal peptide ratio extraction, termed MaxLFQ. *Mol Cell Proteomics* **13**, 2513-2526 (2014). https://doi.org:10.1074/mcp.M113.031591
78 Lu, L. *et al.* Identification of MS-Cleavable and Noncleavable Chemically Cross-Linked Peptides with MetaMorpheus. *J Proteome Res* **17**, 2370-2376 (2018). https://doi.org:10.1021/acs.jproteome.8b00141
79 Chen, Z. L. *et al.* A high-speed search engine pLink 2 with systematic evaluation for proteome-scale identification of cross-linked peptides. *Nat Commun* **10**, 3404 (2019). https://doi.org:10.1038/s41467-019-11337-z
80 Riffle, M., Jaschob, D., Zelter, A. & Davis, T. N. ProXL (Protein Cross-Linking Database): A Platform for Analysis, Visualization, and Sharing of Protein Cross-Linking Mass Spectrometry Data. *J Proteome Res* **15**, 2863-2870 (2016). https://doi.org:10.1021/acs.jproteome.6b00274
81 Jumper, J. *et al.* Highly accurate protein structure prediction with AlphaFold. *Nature* **596**, 583-589 (2021). https://doi.org:10.1038/s41586-021-03819-2
82 Kozakov, D. *et al.* The ClusPro web server for protein-protein docking. *Nat Protoc* **12**, 255-278 (2017). https://doi.org:10.1038/nprot.2016.169
83 Zhou, P., Jin, B., Li, H. & Huang, S. Y. HPEPDOCK: a web server for blind peptide-protein docking based on a hierarchical algorithm. *Nucleic Acids Res* **46**, W443-W450 (2018). https://doi.org:10.1093/nar/gky357
84 Yu, C. *et al.* A mechanism for preventing asymmetric histone segregation onto replicating DNA strands. *Science* **361**, 1386-1389 (2018). https://doi.org:10.1126/science.aat8849
85 Raveh, B., London, N. & Schueler-Furman, O. Sub-angstrom modeling of complexes between flexible peptides and globular proteins. *Proteins* **78**, 2029-2040 (2010). https://doi.org:10.1002/prot.22716
86 Xue, L. C., Rodrigues, J. P., Kastritis, P. L., Bonvin, A. M. & Vangone, A. PRODIGY: a web server for predicting the binding affinity of protein-protein complexes. *Bioinformatics* **32**, 3676-3678 (2016). https://doi.org:10.1093/bioinformatics/btw514
87 Romero-Molina, S. *et al.* PPI-Affinity: A Web Tool for the Prediction and Optimization of Protein-Peptide and Protein-Protein Binding Affinity. *J Proteome Res* **21**, 1829-1841 (2022). https://doi.org:10.1021/acs.jproteome.2c00020
88 Vizcaino, J. A. *et al.* 2016 update of the PRIDE database and its related tools. *Nucleic Acids Res* **44**, D447-456 (2016). https://doi.org:10.1093/nar/gkv1145

Acknowledgements

We thank Nora Cronin, Rebecca Thompson and Daniel Maskell, Yehuda Halfon, Pascale Schelleberger and Fabienne Beuron for assistance with cryo-EM. We also thank Svenja Heimann and Jenny Bormann for technical assistance with crosslinking and APEX2 mass

spectrometry and Ken L. Dreger for our local ProXL server. We further thank Stefan Westermann, Hemmo Meyer and Olaf Stemmann for sharing reagents and expertise on biochemistry and *Xenopus* egg extracts. The lab of D.B. was supported by the CRC1430 and RTG1739 of the DFG and the NRW Rückkehrerförderprogramm (state of North-Rhine-Westphalia), the labs of A.W.O and L.H.P. by Cancer Research UK Programme Grants C302/A14532 and C302/A24386, and the lab of M.R. by the FOR2800 research group (DFG). E.S.G. acknowledges funding from the DFG under Germany´s Excellence Strategy (EXC 2033 – 390677874 – RESOLV), the instrumentation program of the DFG (436586093) and CRC1430. M.K. and F.K. are grateful for funding by the DFG (DFG, INST 20876/322-1 FUGG and CRC1430).

1285 ## Figure Legends

1286

1287 **Figure 1: GINS and TopBP1 interact.**

1288

1289 a: (i) Domain model of human (hs)TopBP1, its conservation with BRCT1/2 and 3/4 domains
1290 (grey boxes) of budding yeast Dpb11 (scDpb11), and interacting proteins. (ii): Overview of
1291 TopBP1 BRCT deletion mutants and respective GINS binding capabilities. Numbers, amino
1292 acid position; capital letters indicate amino acid substitutions.

1293

1294 b: Elution profiles of size exclusion chromatography of individual recombinant TopBP1-
1295 BRCT0-5 protein (grey) and GINS tetramers (green), or of both upon incubation (blue).

1296

1297 c-e: Immobilised recombinant GINS was used to pull down TopBP1-0-5-WT (d), TopBP1-
1298 ΔBRCT3 (e) or TopBP1-ΔBRCT4/5 (f). SDS gels were silver stained.

1299

1300

1301 **Figure 2: Protein structure of the GINS-TopBP1-BRCT4/5 complex.**
1302 a: Model of the GINS-TopBP1-BRCT4/5 complex produced by docking crystal structures of the
1303 GINS complex, and the central BRCT4/5 domain of TopBP1, into the volume determined by
1304 cryo-EM.

1305

1306 b: Zoom-in of the BRCT4-Psf1 interface. The residues in stick representation appear crucial
1307 for the interface. Mutations to break the interaction are coloured pink and purple in Psf1-
1308 I97R and TopBP1-B4mut, respectively.

1309

1310 c: Pulldown of the indicated recombinant TopBP1-BRCT0-5-strep versions by bead-
1311 immobilised GINS. Analysis was done by immunoblotting.

1312

1313 d: Pulldown of the indicated recombinant TopBP1-BRCT0-5-strep versions using immobilised
1314 GINS-WT or GINS carrying a Ile97 to arginine mutation in Psf1.

1315

1316

1317 **Figure 3: The conserved core of the TopBP1-GINI domain is required for a stable interaction**
1318 **with GINS**

1319

1320 a: T-COFFEE alignment of TopBP1 proteins from humans (Q92547) *Xenopus laevis* (Q7ZZY3),
1321 *Bos taurus* (A0A3Q1LWE4) and *Rattus norvegicus* (A0A8I6GFZ6). Amino acid substitutions and
1322 names of GINI core region mutations are shown. Coloured boxes indicate regions I (blue), core
1323 helix (red), regions II (green) and III (orange). GINI-core mutants are shown with their
1324 respective GINS binding capabilities (details in Fig. 3-S1a).

1325

1326 b: Pulldown of the indicated recombinant TopBP1-BRCT0-5-strep versions (Fig. 3-S1a) by
1327 bead-immobilised GINS. Analysis was done by immunoblotting.

1328

1329 c: Fluorescence polarisation experiments using recombinant GINS tetramer and fluorescently
1330 labelled TopBP1-GINI-core (WT or Gpp (panel a)) peptides are shown.

1331

d) Cryo-EM volume showing extra helical density ascribed to the GINI helix (left) alongside a structural model (right) based on this cryo-EM and an AlphaFold2 predicted structure.

e) Pulldown of the indicated recombinant TopBP1-BRCT0-5-strep versions using immobilised GINS-WT or GINS carrying the indicated Psf1 mutations. Analysis was done by immunoblotting.

Figure 4: Both GINS binding surfaces in TopBP1 cooperate in supporting DNA replication.

a: PPI-Affinity and PRODIGY were used to estimate the free energy (in kcal/mol) of the interactions involving TopBP1-GINI and BRCT4.

b: Coomassie-stained SDS PAGE gel of the indicated recombinant TopBP1-BRCT0-5 proteins.

c: The indicated relative amounts (100 % - 10 %) of immunodepleted and non-depleted *Xenopus* egg extracts (Xtract) were analysed by immunoblotting using TopBP1 antibody #2. TopBP1 antibodies #1 and #2 and IgG (mock) were used for immunodepletion. Ponc, ponceau staining.

d/e: Replication analysis of *Xenopus* egg extracts immunodepleted with indicated antibodies upon adding back buffer (buf), or recombinant wild-type (WT) or mutant TopBP1-BRCT0-5-strep shown in b.

Figure 5: GINS binding to TopBP1 is required the origin firing step of replication.

a-c: Label-free quantification of chromatin-bound proteins by mass spectrometry upon chromatin isolation from *Xenopus* egg extracts after replacing endogenous TopBP1 with indicated TopBP1 mutants as described in figure 4. (a) Semi-quantitative heat map, (b) schematic model of DNA replication, (c) volcano plots highlighting a selection of differentially detected proteins (details in Fig. 5-S1).

d: Immunoblot analysis of chromatin-bound proteins upon isolation from *Xenopus* egg extracts as described in a.

Figure 6: Exclusive binding of TopBP1 and DNA polymerase epsilon to GINS in the CMG context.

a: Structure of human CMG with our GINS-TopBP1 superposed to show the binding sites in the context of the CMG

b: CMG-Polε shown from the same angle as CMG-TopBP1 in a demonstrates BRCT4 and PolE2 occupy the same region

c: Closeup of interaction sites on GINS for TopBP1 BRCT4 and PolE2

Figure 1

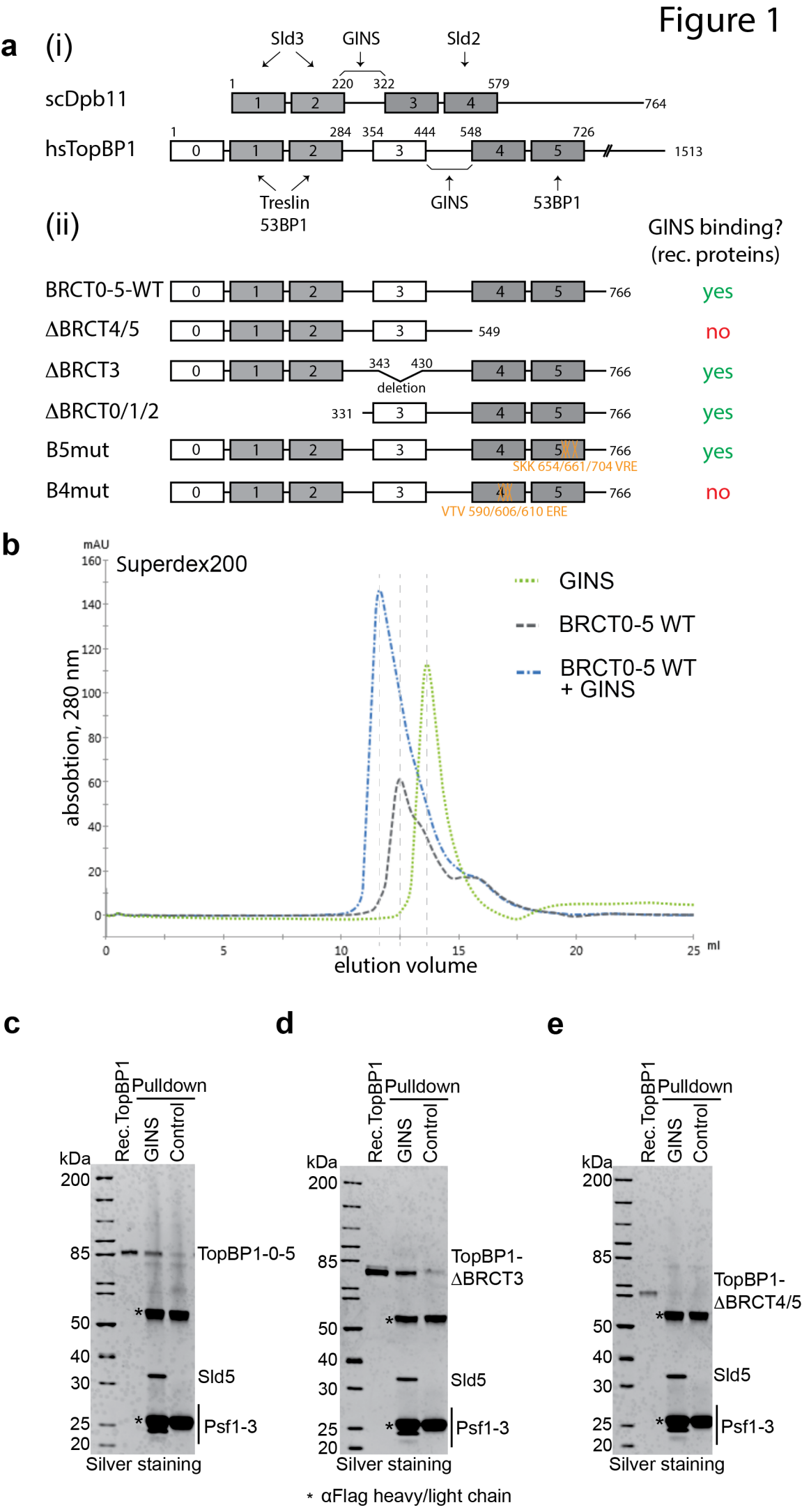
a
(i)
Sld3
GINS
Sld2
scDpb11
1
220
322
579
764
hsTopBP1
1
284
354
444
548
726
1513
Treslin
53BP1
GINS
53BP1
(ii)
GINS binding?
(rec. proteins)
BRCT0-5-WT
766
yes
ΔBRCT4/5
549
no
ΔBRCT3
343
430
deletion
766
yes
ΔBRCT0/1/2
331
766
yes
B5mut
766
SKK 654/661/704 VRE
yes
B4mut
766
VTV 590/606/610 ERE
no
b
Superdex200
mAU
absobtion, 280 nm
elution volume
ml
GINS
BRCT0-5 WT
BRCT0-5 WT
+ GINS
c
d
e
Rec.TopBP1
Pulldown
GINS
Control
kDa
TopBP1-0-5
TopBP1-
ΔBRCT3
TopBP1-
ΔBRCT4/5
Sld5
Psf1-3
Silver staining
* αFlag heavy/light chain

Figure 2

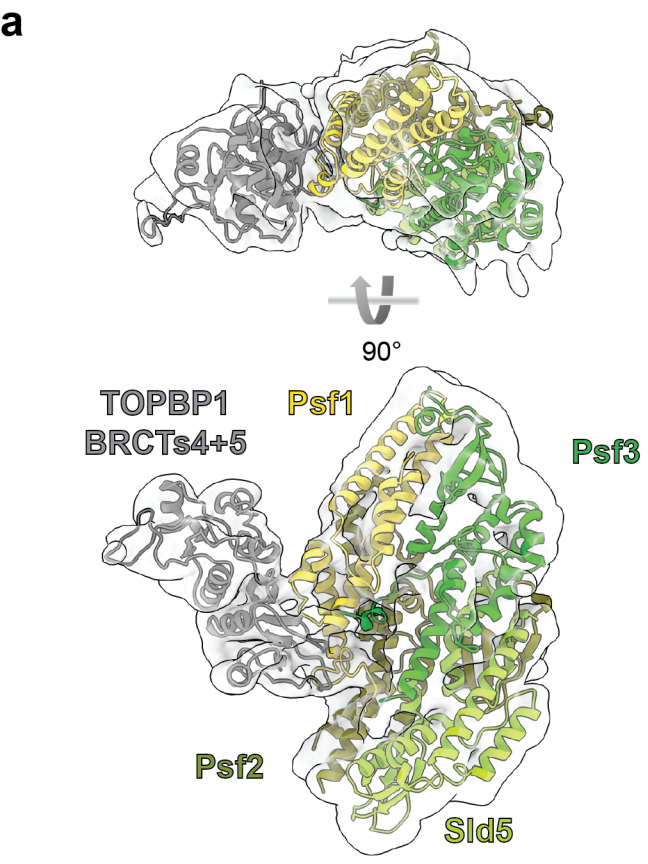
a
90°
TOPBP1
BRCTs4+5
Psf1
Psf3
Psf2
Sld5

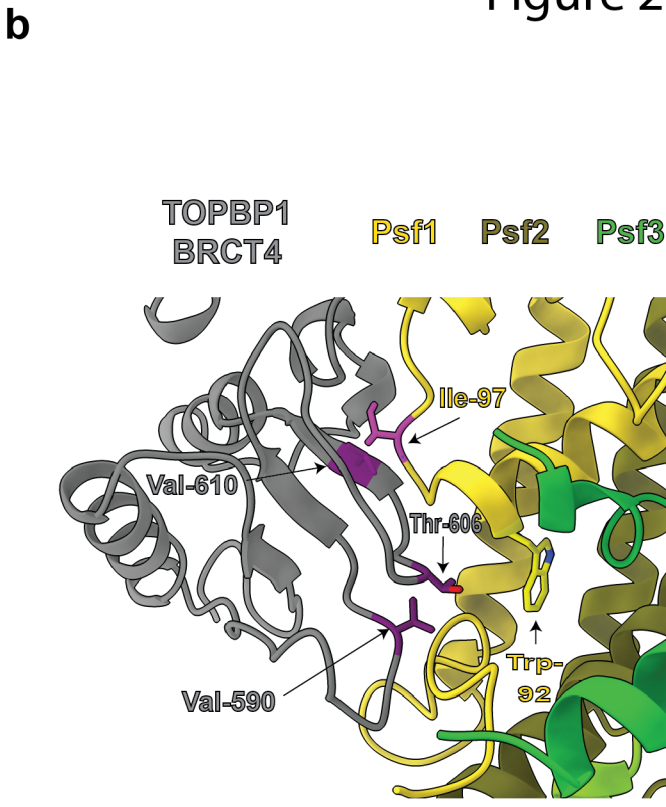
b
TOPBP1
BRCT4
Psf1
Psf2
Psf3
Ile-97
Val-610
Thr-606
Trp-
92
Val-590

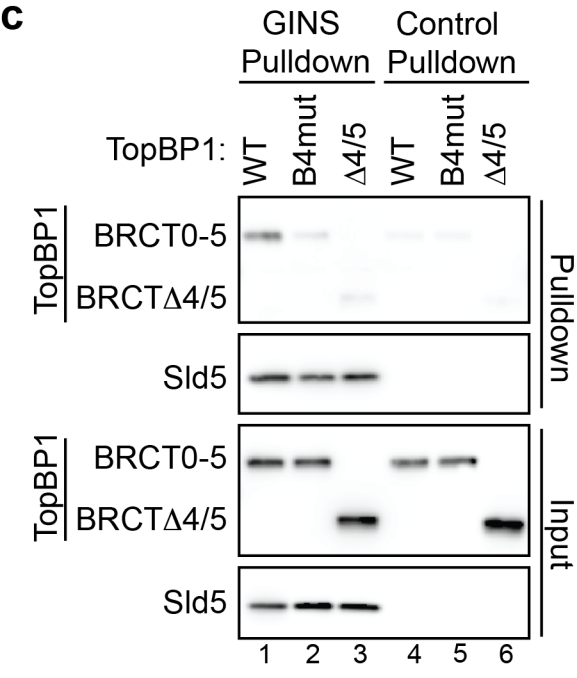
c
GINS
Pulldown
Control
Pulldown
TopBP1:
WT
B4mut
Δ4/5
WT
B4mut
Δ4/5
TopBP1
BRCT0-5
BRCTΔ4/5
Sld5
Pulldown
TopBP1
BRCT0-5
BRCTΔ4/5
Sld5
Input
1
2
3
4
5
6

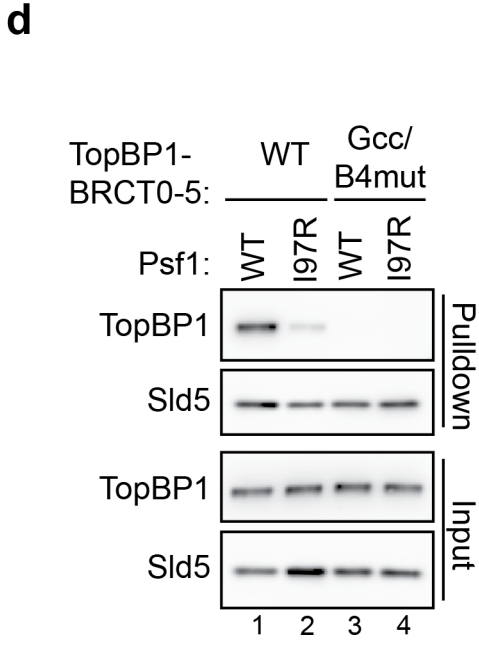
d
TopBP1-
BRCT0-5:
WT
Gcc/
B4mut
Psf1:
WT
I97R
WT
I97R
TopBP1
Sld5
Pulldown
TopBP1
Sld5
Input
1
2
3
4

Figure 3

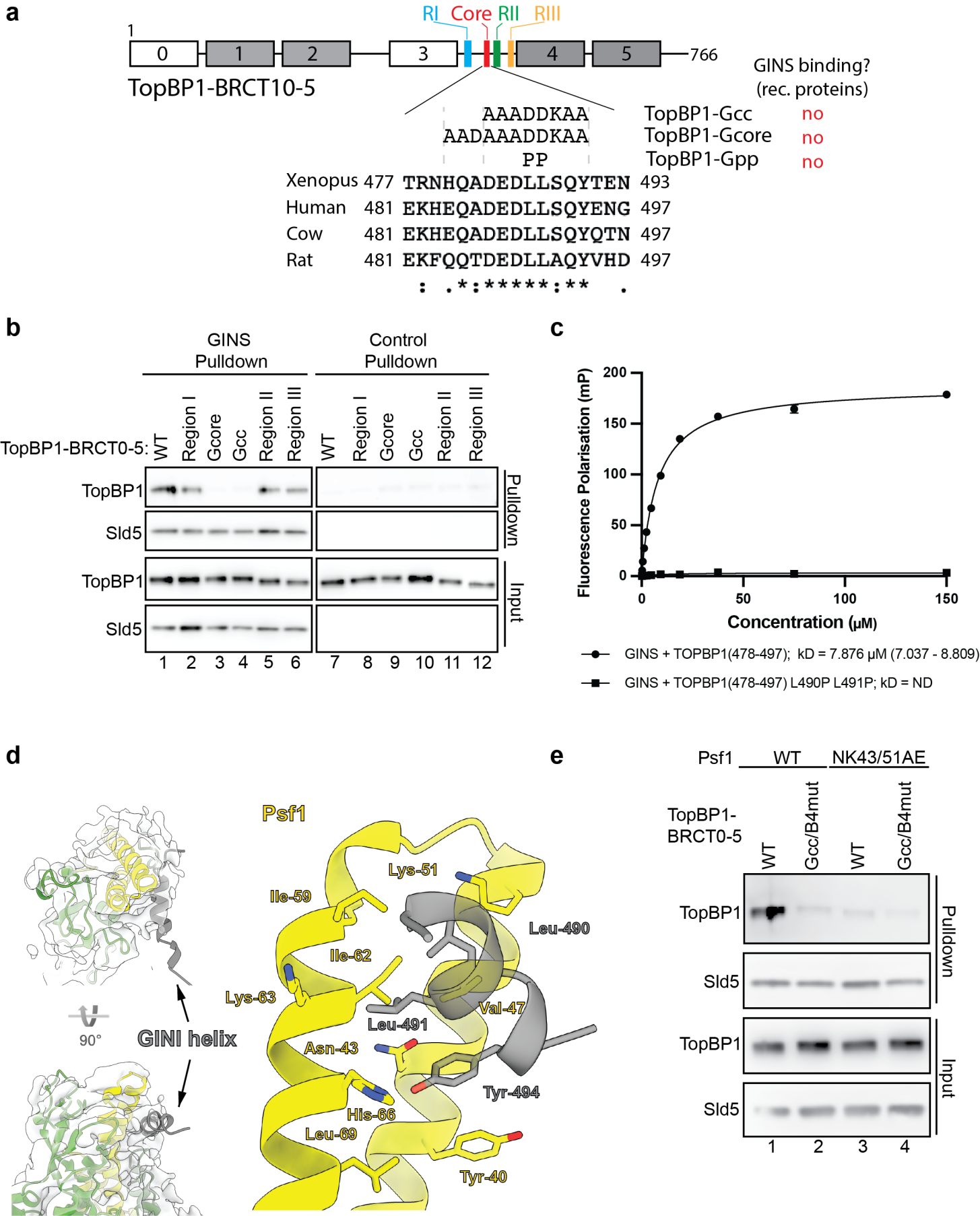
a
RI Core RII RIII
1
0 1 2 3 4 5 766
TopBP1-BRCT10-5
GINS binding?
(rec. proteins)
AAADDKAA
AADAAADDKAA
PP
TopBP1-Gcc no
TopBP1-Gcore no
TopBP1-Gpp no
Xenopus 477 TRNHQADEDLLSQYTEN 493
Human 481 EKHEQADEDLLSQYENG 497
Cow 481 EKHEQADEDLLSQYQTN 497
Rat 481 EKFQQTDEDLLAQYVHD 497
: .*:*****:** .
b
GINS Pulldown
Control Pulldown
TopBP1-BRCT0-5: WT Region I Gcore Gcc Region II Region III WT Region I Gcore Gcc Region II Region III
TopBP1
Sld5
Pulldown
TopBP1
Sld5
Input
1 2 3 4 5 6 7 8 9 10 11 12
c
Fluorescence Polarisation (mP)
200
150
100
50
0
0 50 100 150
Concentration (μM)
GINS + TOPBP1(478-497); kD = 7.876 μM (7.037 - 8.809)
GINS + TOPBP1(478-497) L490P L491P; kD = ND
d
Psf1
Lys-51
Ile-59
Leu-490
Ile-62
Lys-63
Val-47
Leu-491
Asn-43
Tyr-494
His-66
Leu-69
Tyr-40
90°
GINI helix
e
Psf1 WT NK43/51AE
TopBP1-BRCT0-5 WT Gcc/B4mut WT Gcc/B4mut
TopBP1
Sld5
Pulldown
TopBP1
Sld5
Input
1 2 3 4

Figure 4

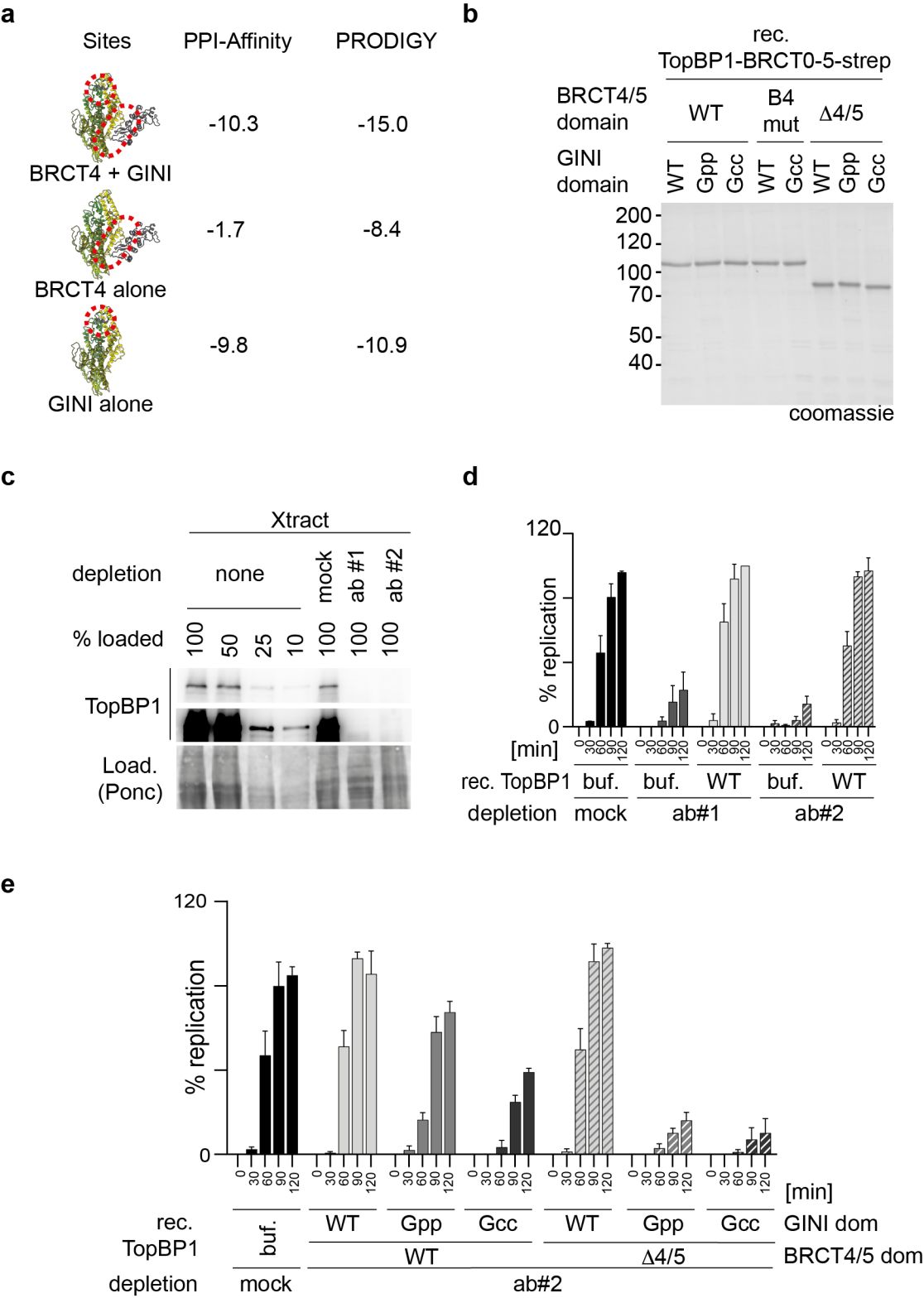
a
Sites
PPI-Affinity
PRODIGY
BRCT4 + GINI
-10.3
-15.0
BRCT4 alone
-1.7
-8.4
GINI alone
-9.8
-10.9
b
rec.
TopBP1-BRCT0-5-strep
BRCT4/5 domain
WT
B4 mut
Δ4/5
GINI domain
WT
Gpp
Gcc
WT
Gcc
WT
Gpp
Gcc
200
120
100
70
50
40
coomassie
c
Xtract
depletion
none
mock
ab #1
ab #2
% loaded
100
50
25
10
100
100
100
TopBP1
Load.
(Ponc)
d
120
% replication
0
[min]
0
30
60
90
120
rec. TopBP1
buf.
buf.
WT
buf.
WT
depletion
mock
ab#1
ab#2
e
120
% replication
0
[min]
rec.
TopBP1
buf.
WT
Gpp
Gcc
WT
Gpp
Gcc
GINI dom
WT
Δ4/5
BRCT4/5 dom
depletion
mock
ab#2

Figure 5

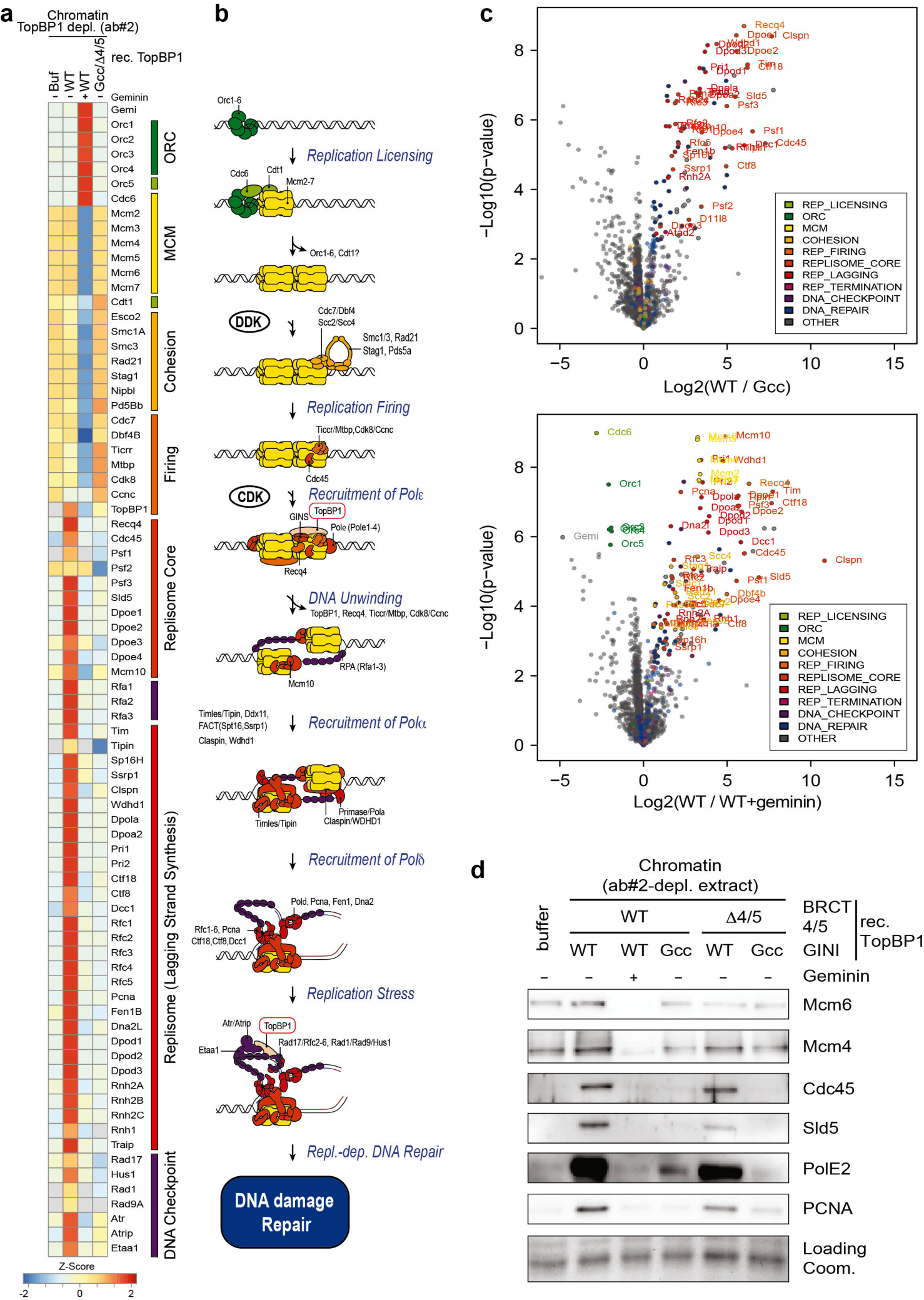
a
Chromatin
TopBP1 depl. (ab#2)
rec. TopBP1
- Buf
- WT
+ WT
- Gcc/Δ4/5
Geminin
Gemi
Orc1
Orc2
Orc3
Orc4
Orc5
Cdc6
Mcm2
Mcm3
Mcm4
Mcm5
Mcm6
Mcm7
Cdt1
Esco2
Smc1A
Smc3
Rad21
Stag1
Nipbl
Pd5Bb
Cdc7
Dbf4B
Ticrr
Mtbp
Cdk8
Ccnc
TopBP1
Recq4
Cdc45
Psf1
Psf2
Psf3
Sld5
Dpoe1
Dpoe2
Dpoe3
Dpoe4
Mcm10
Rfa1
Rfa2
Rfa3
Tim
Tipin
Sp16H
Ssrp1
Clspn
Wdhd1
Dpola
Dpoa2
Pri1
Pri2
Ctf18
Ctf8
Dcc1
Rfc1
Rfc2
Rfc3
Rfc4
Rfc5
Pcna
Fen1B
Dna2L
Dpod1
Dpod2
Dpod3
Rnh2A
Rnh2B
Rnh2C
Rnh1
Traip
Rad17
Hus1
Rad1
Rad9A
Atr
Atrip
Etaa1
ORC
MCM
Cohesion
Firing
Replisome Core
Replisome (Lagging Strand Synthesis)
DNA Checkpoint
Z-Score
-2
0
2
b
Orc1-6
Replication Licensing
Cdc6
Cdt1
Mcm2-7
Orc1-6, Cdt1?
DDK
Cdc7/Dbf4
Scc2/Scc4
Smc1/3, Rad21
Stag1, Pds5a
Replication Firing
Ticcr/Mtbp,Cdk8/Ccnc
Cdc45
CDK
Recruitment of Polε
GINS
TopBP1
Pole (Pole1-4)
Recq4
DNA Unwinding
TopBP1, Recq4, Ticcr/Mtbp, Cdk8/Ccnc
RPA (Rfa1-3)
Mcm10
Timles/Tipin, Ddx11,
FACT(Spt16,Ssrp1)
Claspin, Wdhd1
Recruitment of Polα
Timles/Tipin
Primase/Pola
Claspin/WDHD1
Recruitment of Polδ
Pold, Pcna, Fen1, Dna2
Rfc1-6, Pcna
Ctf18,Ctf8,Dcc1
Replication Stress
Atr/Atrip
TopBP1
Etaa1
Rad17/Rfc2-6, Rad1/Rad9/Hus1
Repl.-dep. DNA Repair
DNA damage
Repair
c
−Log10(p−value)
Log2(WT / Gcc)
REP_LICENSING
ORC
MCM
COHESION
REP_FIRING
REPLISOME_CORE
REP_LAGGING
REP_TERMINATION
DNA_CHECKPOINT
DNA_REPAIR
OTHER
Log2(WT / WT+geminin)
d
Chromatin
(ab#2-depl. extract)
buffer
WT
Δ4/5
BRCT 4/5
GINI
rec. TopBP1
WT
WT
Gcc
WT
Gcc
Geminin
Mcm6
Mcm4
Cdc45
Sld5
PolE2
PCNA
Loading
Coom.

Figure 6

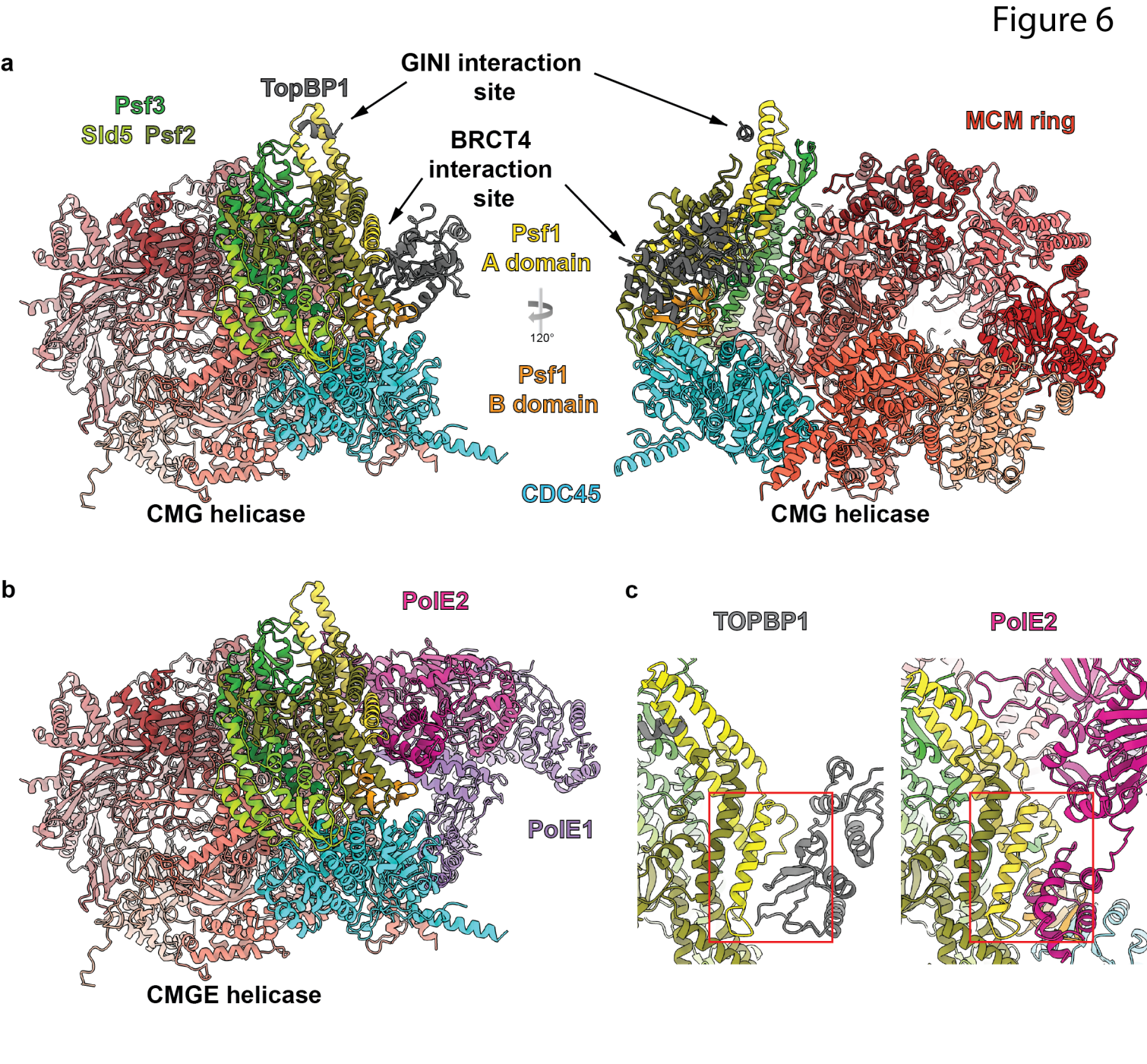
a
GINI interaction site
TopBP1
Psf3
Sld5 Psf2
BRCT4 interaction site
MCM ring
Psf1 A domain
120°
Psf1 B domain
CDC45
CMG helicase
CMG helicase
b
PolE2
PolE1
CMGE helicase
c
TOPBP1
PolE2